

REPORT DOCUMENTATION PAGE			Form Approved OMB No. 074-0188	
Public reporting burden for this collection of information is estimated to average 1 hour per response, including the time for reviewing instructions, searching existing data sources, gathering and maintaining the data needed, and completing and reviewing this collection of information. Send comments regarding this burden estimate or any other aspect of this collection of information, including suggestions for reducing this burden to Washington Headquarters Services, Directorate for Information Operations and Reports, 1215 Jefferson Davis Highway, Suite 1204, Arlington, VA 22202-4302, and to the Office of Management and Budget, Paperwork Reduction Project (0704-0188), Washington, DC 20503				
1. AGENCY USE ONLY		2. REPORT DATE 6/29/98	3. REPORT TYPE AND DATES COVERED Technical Report, Oct 1996 - June 1998	
4. TITLE AND SUBTITLE New Organic-Inorganic Nanocomposite Materials for Energy Storage Applications			5. FUNDING NUMBERS N00014-96-1-0673 96PR0-3839	
6. AUTHOR(S) E. Shouji and D. A. Buttry				
7. PERFORMING ORGANIZATION NAME(S) AND ADDRESS(ES) Department of Chemistry University of Wyoming Laramie, Wyoming 82071-3838			8. PERFORMING ORGANIZATION REPORT NUMBER Technical Report 40	
9. SPONSORING / MONITORING AGENCY NAME(S) AND ADDRESS(ES) Office of Naval Research, ONR 331 800 North Quincy Street Arlington, VA 22217-5660			10. SPONSORING / MONITORING AGENCY REPORT NUMBER	
11. SUPPLEMENTARY NOTES Prepared for publication in <i>Langmuir</i>				
12a. DISTRIBUTION / AVAILABILITY STATEMENT This document has been prepared for public release and sale; its distribution is unlimited.				12b. DISTRIBUTION CODE
13. ABSTRACT ( <i>Maximum 200 Words</i> ) A method is described by which the disulfide dimer of 2,5-dimercapto-1,3,4-thiadiazole (diDMcT, see Scheme 1) can be oxidatively intercalated into the layered structure of a V <sub>2</sub> O <sub>5</sub> xerogel. This intercalation reaction produces a new organic-inorganic composite material with a layer spacing of 13.5 Å, in contrast to the 11.55 Å spacing for the parent V <sub>2</sub> O <sub>5</sub> xerogel. During this oxidative intercalation, the diDMcT is polymerized to produce a polymer with thiadiazole rings linked by disulfides in the polymer main chain (PDTT, see Scheme 1). The composite material is characterized by uv-visible spectroelectrochemistry, x-ray diffraction, FTIR and electrochemistry. The electrochemical experiments comprised charging (oxidation) and discharging (reduction) of the material, with the bulk of the redox reaction occurring over a broad potential range of 0.5 V to -0.6 V versus SCE. The cyclic voltammogram of the composite material shows features that can be attributed to the DMcT-PDTT redox response. However, during or after reduction of the composite, the monomeric DMcT dithiolate appears to be expelled from the V <sub>2</sub> O <sub>5</sub> interlayer region, leading to an evolution of the electrochemical response back to that of the original V <sub>2</sub> O <sub>5</sub> material. Evidence is presented suggesting that the V <sub>2</sub> O <sub>5</sub> host material facilitates the redox reactions of the thiol-disulfide redox couple while it is within the interlayer region.				
14. SUBJECT TERMS lithium secondary battery, cathode, intercalation			15. NUMBER OF PAGES 33	
			16. PRICE CODE	
17. SECURITY CLASSIFICATION OF REPORT unclassified	18. SECURITY CLASSIFICATION OF THIS PAGE unclassified	19. SECURITY CLASSIFICATION OF ABSTRACT unclassified	20. LIMITATION OF ABSTRACT	
NSN 7540-01-280-5500			Standard Form 298 (Rev. 2-89) Prescribed by ANSI Std. Z39-18 298-102	

19980710052

OFFICE OF NAVAL RESEARCH

GRANT # N00014-91-J-0201

R&T CODE: 4133032

Technical Report No. 40

New Organic-Inorganic Nanocomposite Materials for Energy Storage Applications

E. Shouji and D. A. Buttry

Prepared for publication

in

*Langmuir*

Department of Chemistry  
University of Wyoming  
Laramie, Wyoming 82071-3838

June 29, 1998

Reproduction in whole, or in part, is permitted for any purpose of the United States Government

This document has been approved for public release and sale; its distribution is unlimited.

REPORT DOCUMENTATION PAGE

2. June 29, 1998

3. Technical Report

4. "New Organic-Inorganic Nanocomposite Materials for Energy Storage Applications"

5. GRANT: N00014-96-1-0673, PR # 96PRO-3839

6. E. Shouji and D. A. Buttry

7. Department of Chemistry, University of Wyoming, Laramie, Wyoming 82071-3838

8. Org. Report # - none

9. Office of Naval Research, Chemistry Division, 800 N. Quincy Street, Arlington, VA 22217-5660

10. Technical Report No. 40

11. Submitted to: *Langmuir*

12. Unlimited distribution

13. Abstract: A method is described by which the disulfide dimer of 2,5-dimercapto-1,3,4-thiadiazole (diDMcT, see Scheme 1) can be oxidatively intercalated into the layered structure of a  $V_2O_5$  xerogel. This intercalation reaction produces a new organic-inorganic composite material with a layer spacing of 13.5 Å, in contrast to the 11.55 Å spacing for the parent  $V_2O_5$  xerogel. During this oxidative intercalation, the diDMcT is polymerized to produce a polymer with thiadiazole rings linked by disulfides in the polymer main chain (PDTT, see Scheme 1). The composite material is characterized by uv-visible spectroelectrochemistry, x-ray diffraction, FTIR and electrochemistry. The electrochemical experiments comprised charging (oxidation) and discharging (reduction) of the material, with the bulk of the redox reaction occurring over a broad potential range of 0.5 V to -0.6 V versus SCE. The cyclic voltammogram of the composite material shows features that can be attributed to the DMcT-PDTT redox response. However, during or after reduction of the composite, the monomeric DMcT dithiolate appears to be expelled from the  $V_2O_5$  interlayer region, leading to an evolution of the electrochemical response back to that of the original  $V_2O_5$  material. Evidence is presented suggesting that the  $V_2O_5$  host material facilitates the redox reactions of the thiol-disulfide redox couple while it is within the interlayer region.

15. Number of Pages: 33

16. Price Code: UL

17. 18. 19. Unclassified

20. Limitations: UL

# New Organic-Inorganic Nanocomposite Materials for Energy

## Storage Applications

Eiichi Shouji and Daniel A. Buttry\*

Department of Chemistry

University of Wyoming

Laramie, WY 82071-3838

*Buttry@uwyo.edu*

*Submitted to  
Energy Storage*

### Abstract

A method is described by which the disulfide dimer of 2,5-dimercapto-1,3,4-thiadiazole (diDMcT, see Scheme 1) can be oxidatively intercalated into the layered structure of a  $V_2O_5$  xerogel. This intercalation reaction produces a new organic-inorganic composite material with a layer spacing of 13.5 Å, in contrast to the 11.55 Å spacing for the parent  $V_2O_5$  xerogel. During this oxidative intercalation, the diDMcT is polymerized to produce a polymer with thiadiazole rings linked by disulfides in the polymer main chain (PDTT, see Scheme 1). The composite material is characterized by uv-visible spectroelectrochemistry, x-ray diffraction, FTIR and electrochemistry. The electrochemical experiments comprised charging (oxidation) and discharging (reduction) of the material, with the bulk of the redox reaction occurring over a broad potential range of 0.5 V to -0.6 V versus SCE. The cyclic voltammogram of the composite material shows features that can be attributed to the DMcT-PDTT redox response. However, during or after reduction of the composite, the monomeric DMcT dithiolate appears to be expelled from the  $V_2O_5$  interlayer region, leading to an evolution of the electrochemical response back to that of the original  $V_2O_5$  material. Evidence is presented suggesting that the  $V_2O_5$  host material facilitates the redox reactions of the thiol-disulfide redox couple while it is within the interlayer region.

### Introduction

Materials that are capable of rapid and efficient charge storage and delivery (i.e. rechargeable redox couples) are important in a host of applications. In many cases, these materials are optimized for a particular aspect of their behavior. For example, the inorganic oxides that have been widely used as Li secondary battery cathode materials<sup>1-4</sup> have good

stability toward long term cycling and fairly positive redox potentials. On the other hand, they suffer from energy densities that are well below those that can be attained with available anodes, and they have relatively low power densities.<sup>1-4</sup> These detrimental characteristics have driven a high level of recent activity in the development of new cathode materials.<sup>4-12</sup> One of the materials that has emerged as having an attractive combination of properties is  $V_2O_5$ . Both high energy density and good reversibility have been demonstrated for this material,<sup>9-12</sup> especially in its aerogel form.<sup>9,11,12</sup>

In battery applications, discharge (reduction) of these materials is accompanied by  $Li^+$  insertion, which is often rate-limiting.<sup>4</sup> Thus, a common strategy to achieve higher discharge rates is to use high surface area materials, so that the distance over which  $Li^+$  must diffuse through the host material is minimized.<sup>9,11,13</sup> Another approach that does not appear to have been explored yet is to manipulate the interlayer spacing in these layered materials by using various intercalants so as to enhance the rate of  $Li^+$  migration. It is well known that intercalation leads to changes in the interlayer spacing for layered materials.<sup>14-19</sup> Examples of such intercalants include thiophene, pyrrole and aniline, all of which are known to oxidatively polymerize when intercalated into highly oxidizing materials such as  $V_2O_5$ .<sup>20-27</sup> Much of the previous work has focussed on electronic and optical properties of the resulting “nanocomposites.” However, little has been done on the influence of intercalation on the redox reactions of either the host material or the intercalant. One goal of our research effort is to examine these effects, especially with regard to the influence of intercalants on  $Li^+$  diffusion rates and charge capacity in these nanocomposites.

In the present case, the intercalant that has been investigated comprises 2,5-dimercapto-1,3,4-thiadiazole (DMcT) in its various monomeric and oligomeric redox forms. Scheme 1 shows the various redox states of DMcT. As has been previously discussed,<sup>37,39</sup> the first oxidation product of DMcT is diDMcT (reaction 1). This disulfide dimer can be oxidatively polymerized to produce PDTT, which is an oligomeric material of undefined degree of polymerization and very low solubility in most common solvents. This material was originally investigated for charge storage purposes by De Jonghe, Visco and coworkers.<sup>28,29</sup> They found it to be unsuitable for use at ambient temperatures because of

sluggishness of the thiol-disulfide redox couple. However, more recently, Oyama and coworkers found that its redox reactions could be "facilitated" by making molecularly mixed composites of DMcT and poly(aniline).<sup>30-38</sup> In order to better understand this phenomenon, we have recently conducted several detailed mechanistic and spectroscopic studies of the redox behavior of DMcT and several of its derivatives, including studies of its acid-base reactions.<sup>37,39</sup> These studies have suggested that the facilitation of DMcT redox cycling is likely a result of proton transfer between poly(aniline) and the DMcT oligomer (PPDT, see Scheme 1). This is especially true during reduction, where it is believed that the availability of protons (from poly(aniline)) drives reductive cleavage of the S-S bond at less negative potentials than would otherwise be observed. In this regard, one of the motivations of the present study was to examine whether or not such redox facilitation could be achieved by using transition metal centers in host materials such as V<sub>2</sub>O<sub>5</sub>. As will be seen below, in spite of long term instability of the PDDT-V<sub>2</sub>O<sub>5</sub> composite with respect to loss of DMcT, there is evidence for this facilitation by the host material, suggesting that similar strategies with other materials might be worthy of additional investigation.

## Experimental

### Materials

All chemicals were of reagent grade or better and were used as received. Acetonitrile (ACN) was freshly distilled from P<sub>2</sub>O<sub>5</sub> prior to use. The vanadium oxide xerogel solution was produced as previously described by ion exchange of NaVO<sub>3</sub> to produce HVO<sub>3</sub>, followed by aging for at least two weeks.<sup>40-42</sup> This procedure produces a viscous, deep wine red solution. DiDMcT was prepared by slow air oxidation of DMcT in ethanol/water (50/50 v/v), producing lemon yellow crystalline needles (yield = 89%). Crystallization started after about 20 hours, and the reaction mixture was left for three days prior to harvesting the crystals. Elemental analysis gave: (formula: C<sub>4</sub>H<sub>2</sub>N<sub>4</sub>S<sub>6</sub>) calculated: H 0.68, C 16.11, N 18.8, S 64.4, observed: H 0.68, C 16.19, N 18.78, S 64.35. The structure was confirmed by x-ray diffraction (see supplementary material), and shows that diDMcT exists in the thioamide tautomer (as opposed to the dithiol tautomer shown in Scheme 1) in the solid state.<sup>37,39</sup>

### *Equipment and procedures*

UV-vis spectroscopic measurements were made using a HP 8452 diode array spectrometer with optically transparent indium-doped tin oxide (ITO) electrodes (Delta Technologies). Electrochemical measurements were made using a PAR 273. X-ray diffraction was done on a Scintag XDS2000 using the following conditions: Cu K $\alpha$ , 40 KV, 30 mA, continuous scan, 1° 2 $\theta$ /min, 0.01° 2 $\theta$ /increment (0.60 seconds/point). Spin coating of the neat gel solution was done using a locally modified unit at a rotation rate of 5000 RPM. FTIR transmission measurements were made on a Bomem MB100 after pressing the samples in KBr pellets.

Films cast onto various electrode substrates had relatively poor adhesion unless the film thickness was kept below ca. 1500 Å. For this reason and to achieve better film uniformity and homogeneity, a spin coating procedure was developed. Spin coated films were prepared on either ITO electrodes or on vapor deposited thin film Au electrodes (2000 Å in thickness, electrode area of 0.34 cm<sup>2</sup>) and dried at 120° C for 20 hours at 0.75 atm (ambient pressure), producing a dark red film. Films prepared in this way were stable for over 50 cyclic voltammetric cycles before adhesive failure led to film delamination. Film thicknesses were typically 1500 Å and were measured on a Rudolph AutoEl II ellipsometer at a wavelength of 632.8 nm using the following values for refractive index: 1.76 (real part) and 0.0 (imaginary part), which are values for crystalline V<sub>2</sub>O<sub>5</sub>.<sup>43</sup> Because the refractive index values for V<sub>2</sub>O<sub>5</sub> xerogels have not been reported, we consider the film thicknesses obtained in this way as fairly rough estimates. Note that the lack of absorption of the V<sub>2</sub>O<sub>5</sub> films at 632.8 nm (see below) supports the use of 0.0 for the imaginary part of the refractive index.

DiDMcT was oxidatively intercalated into V<sub>2</sub>O<sub>5</sub> by exposing V<sub>2</sub>O<sub>5</sub> films (prepared as described above) to 5 mM ACN solutions of diDMcT for 48 hours at reflux. Oxidative intercalation of diDMcT and simultaneous reduction of vanadium sites in the host material were characterized by a color change of the film from deep red to dark green, as expected for reduction of V(V) to V(IV).<sup>42</sup> Initial experiments using DMcT as the intercalant

produced composite films that had very poor redox and adhesive properties. We suspect this is due to the strongly acidic nature of DMcT ( $\text{p}K_{\text{a}1} = -1.36$ ),<sup>37</sup> which may adversely affect the  $\text{V}_2\text{O}_5$  host material. Thus, all experiments were done with composite films produced by oxidative intercalation of diDMcT into  $\text{V}_2\text{O}_5$ . As noted above, for short term experiments (i.e. less than 50 scans) the adhesion of these films to ITO or Au electrodes was not adversely affected by the dimensional changes accompanying the intercalation (see below), so long as the film thickness was ca. 1500 Å or less.

The supporting electrolyte for all experiments was 0.2 M  $\text{LiClO}_4$  in ACN. Cyclic voltammetric experiments with diDMcT and DMcT in 0.2 M  $\text{LiClO}_4/\text{ACN}$  solution were made using a glassy carbon working electrode with an area of 0.0707  $\text{cm}^2$ , a Pt counter electrode and a Ag/AgCl reference electrode, with respect to which all potentials are reported. Solutions were thoroughly purged with Ar prior to all experiments.

## Results and Discussion

Figure 1a shows the results of a spectroelectrochemical experiment in which a thin film of  $\text{V}_2\text{O}_5$  on an ITO substrate was sequentially exposed to potentials between 1.3 V and -0.2 V. Reduction of the V(V) sites in the lattice to V(IV) leads to loss of the strong band at 385 nm and simultaneous appearance of a broad, weaker long wavelength band with  $\lambda_{\text{max}}$  near 750 nm. These data are entirely consistent with previous observations of the spectral changes accompanying redox reactions of these materials.<sup>42</sup> Figure 1b (curve b) shows the uv-vis spectrum that is observed when a  $\text{V}_2\text{O}_5$  film on an ITO substrate is exposed to a diDMcT solution in ACN. Reaction results in loss of the strong 385 nm band and the appearance of weak absorbance in the long wavelength region above 500 nm. These spectral changes are consistent with the reduction of V(V) to V(IV) during exposure to diDMcT. Based on these results, it is reasonable to assume that diDMcT must be oxidized during this process. Unfortunately, the uv cutoff of the ITO substrate does not allow direct observation of the spectral changes that should accompany this oxidation.<sup>37, 39</sup>

FTIR characterization of  $\text{V}_2\text{O}_5$  films before and after exposure to diDMcT is also helpful in diagnosing the reaction between them. Figures 2a and 2b show the infrared

spectra of diDMcT and PDTT, respectively. As can be seen, both compounds show strong bands near  $1050\text{ cm}^{-1}$  and  $1380\text{ cm}^{-1}$ . However, they can be distinguished from each other by virtue of the presence of a strong doublet in the  $1275\text{ cm}^{-1}$  region for diDMcT and the lack of any significant bands in this region for PDTT. Assignment of the infrared and Raman spectra for these compounds is the subject of an impending contribution,<sup>44</sup> and is not necessary for the purposes of the present investigation. Figure 2c shows the spectrum of a  $\text{V}_2\text{O}$  sample. The V-O-V and V=O bands at ca.  $800\text{ cm}^{-1}$  and  $1050\text{ cm}^{-1}$ , respectively, are characteristic of this material,<sup>43</sup> as is the weak band at  $1640\text{ cm}^{-1}$  showing the presence of some residual water in the sample.<sup>43</sup> Figure 2d shows the spectrum that is obtained for a  $\text{V}_2\text{O}_5$  sample that was exposed to 5 mM diDMcT in ACN at reflux for 48 hours. This spectrum very clearly shows that the sample contains a large amount of PDTT, based on the presence of strong bands near  $1050\text{ cm}^{-1}$  and  $1380\text{ cm}^{-1}$ , and no diDMcT, based on the complete absence of any bands in the  $1275\text{ cm}^{-1}$  region. The ratio of the PDTT band intensities to those for the  $\text{V}_2\text{O}_5$  component of the sample suggests that the sample contains a relatively large amount of PDTT relative to  $\text{V}_2\text{O}_5$ . It is possible to use time and temperature to control the amount of PDTT produced by this reaction. For example, exposure for 48 hours at ambient temperature, rather than at reflux, produces a sample that has relatively weaker PDTT bands and relatively stronger  $\text{V}_2\text{O}_5$  bands (data not shown). Based on previous reports that  $\text{V}_2\text{O}_5$  is swollen by ACN at reflux temperatures,<sup>23</sup> these results suggest that the amount of PDTT produced in this reaction is determined by how the reaction conditions influence access of diDMcT to the interior of the  $\text{V}_2\text{O}_5$  layers.

X-ray diffraction of spin coated films of  $\text{V}_2\text{O}_5$  and PDTT- $\text{V}_2\text{O}_5$  shows prominent reflections at  $2\theta$  values that give lattice spacings of  $11.55\text{ \AA}$  and  $13.5\text{ \AA}$ , respectively (data not shown). This value for the  $\text{V}_2\text{O}_5$  xerogel is consistent with previous observations for this material, and suggests that the films produced by the spin coating-heat treatment procedure described in the Experimental section results in  $\text{V}_2\text{O}_5 \cdot 1.5\text{ H}_2\text{O}$ .<sup>40-42</sup> The value for the PDTT- $\text{V}_2\text{O}_5$  samples is consistent with the premise that the PDTT is intercalated into the interlayer region of the  $\text{V}_2\text{O}_5$  host lattice, based on previous observations of changes in layer spacing on intercalation of other planar organic compounds into layered materials.<sup>18-27</sup> Interestingly, the XRD data for the PDTT- $\text{V}_2\text{O}_5$  sample do not show a peak corresponding to

the 11.55 Å spacing, suggesting that the intercalation reaction is complete and that none of the  $V_2O_5$  parent material remains after reaction. Thus, taken together, the data suggest that the reaction between diDMcT and  $V_2O_5$  produces a material with a structure such as that schematically depicted in Scheme 2, in which the PDTT oligomers are intercalated into the interlayer region of the  $V_2O_5$  host lattice and the planes of the thiadiazole rings are nearly parallel with the  $V_2O_5$  layers. A non-parallel orientation of the thiadiazole rings would not be consistent with the layer spacing of 13.5 Å. In this regard, it is interesting that the crystal structure of diDMcT (see supplementary material) shows the C-S-S-C dihedral angle to be 92°, as expected. Additionally, the angle between the planes of the two thiadiazole rings in each dimer is ca. 90°. This geometry leads to unit cell dimensions of 5.72 Å x 5.92 Å x 15.89 Å, with the two shorter dimensions being roughly determined by the distance across the two thiadiazole rings. As mentioned above, such a geometry would *not* be consistent with the interlayer spacing of 13.5 Å for the PDTT- $V_2O_5$  composite, suggesting that the angle between the two thiadiazole rings in this material must be considerably less than 90°.

Figure 3a shows a cyclic voltammetric experiment for a  $V_2O_5$  thin film on a vapor deposited Au electrode. The broad cathodic and anodic waves in the range 0.5 V to -0.6 V result from the reduction and oxidation, respectively, of V sites in the lattice. These data are in excellent agreement with previous reports on  $V_2O_5$  xerogels.<sup>9-11</sup> A detailed analysis of the voltammetry of  $V_2O_5$  xerogels is not attempted here, being unnecessary for the purposes of the present discussion. Figure 3b (solid curve) shows the first reductive scan for a PDTT- $V_2O_5$  thin film. The salient feature is a much larger cathodic current at ca. -0.1 V compared to the response of the  $V_2O_5$  xerogel parent material. Some of this cathodic charge is recovered in the same potential range during the positive-going, return scan. We attribute this excess charge to the reduction and reoxidation of some of the PDTT material that is present within the interlayer region. This charge is considerably diminished in the second scan (dashed curve) and continues diminishing during subsequent scans. With continuous scanning, the voltammetry of the system slowly (ca. 1 hour) evolves back to that of the  $V_2O_5$  xerogel parent material. This suggests that some amount of the DMcT (which most likely will be present as the dithiolate<sup>37-39</sup>) that is produced on reduction of the PDTT oligomer

diffuses out of the  $V_2O_5$  host lattice during each scan. After many scans, the voltammetry indicates that most of the DMcT/PDcT intercalated material has been lost from the  $V_2O_5$  thin film.

It is interesting to compare the behavior of the DMcT-PDcT redox couple within the  $V_2O_5$  lattice to that observed for diDMcT and DMcT in solution. Figure 4 shows the cyclic voltammetry for a diDMcT sample in ACN solution. This compound shows a cathodic peak at  $-0.2$  V which corresponds to reductive cleavage of the S-S bond in diDMcT to give the monothiolate form of DMcT.<sup>37,39</sup> The anodic peak at  $0.15$  V corresponds to reoxidation of the DMcT monothiolate to give diDMcT.<sup>37,39</sup> The situation is more complex for DMcT, due in large measure to polymerization-depolymerization processes and proton transfer that occur during the redox transitions.<sup>37,39,45</sup> Figure 5a shows the voltammetry for a solution of DMcT at a scan rate of  $200$   $\text{mV s}^{-1}$ . At this scan rate extensive precipitation and corresponding complications in the voltammetry are somewhat avoided; lower scan rates lead to much more complex voltammetry. The salient feature of Figure 5a are the peaks for DMcT oxidation at potentials in the range  $0.8$  V to  $1.2$  V and for the corresponding reduction at  $-0.4$  V. This oxidation potential is that observed for the neutral, fully protonated form of DMcT.<sup>37,39,45</sup> Note that it is nearly a volt more positive than that for the oxidation of the DMcT monothiolate form, showing the very strong influence of proton availability (or lack of it) on redox potentials in this non-aqueous solvent system. The subsequent reduction is that observed for direct, “unassisted” (meaning unassisted by protons, see below) reductive cleavage of the S-S bond in PDcT. Figure 5b shows the cyclic voltammetric response that is observed when a strong acid (trifluoromethane sulfonic acid, TFMSA) is added to the solution. The important feature to note is the appearance of a new, less negative reduction wave at ca.  $0.0$  V. As has been established in other studies, this wave corresponds to the proton assisted (or facilitated) reductive cleavage of the S-S bond.<sup>37,39,45</sup> Comparison of the potential for PDcT reduction in the presence of protons with that for PDcT reduction in the  $V_2O_5$  lattice reveals a good correspondence between the two. It is especially significant that these reductions occur ca.  $0.3$  V less negative than that for the unassisted reductive cleavage of the S-S bond in PDcT. This suggests that the metal

centers in the  $V_2O_5$  lattice may act in a manner similar to that of protons in terms of facilitating the S-S reductive cleavage.

## Conclusions

This study has revealed that diDMcT can be oxidatively intercalated into the interlayer region of a  $V_2O_5$  xerogel host lattice, as confirmed by uv-vis and FTIR spectroscopic studies, x-ray diffraction and electrochemical experiments. This redox reaction produces a material whose composition is consistent with an organic-inorganic composite that can be formulated as  $(PDTT)_x-(V_2O_5)_y$ , where  $x$  and  $y$  can be controlled by the reaction conditions. While intercalation is relatively facile and can be driven to high levels, the electrochemical behavior of the composite material during redox cycling suggests that DMcT is lost from the  $V_2O_5$  interlayer region while in its reduced form, most likely due to diffusion out of the lattice. This may not be unexpected, given the electrostatic repulsion expected between the negatively charged, reduced  $V_2O_5$  lattice<sup>40-42</sup> and the monothiolate or dithiolate forms of DMcT (which are the most likely forms to exist under these conditions).<sup>37,39</sup> However, in spite of this loss of intercalant, the suggestion that the V centers may be facilitating the S-S reductive cleavage indicates that further studies of composite materials of S-containing guests in transition metal hosts may be worthwhile. This is especially true since the kinetics, rather than the thermodynamics, of the thiol-disulfide redox transformations appear to be the stumbling block for their use in redox cycling applications.<sup>28,29</sup>

**Acknowledgment.** This work was supported in full by the Office of Naval Research. We are grateful to Prof. Bruce Dunn (UCLA) for a preprint of his work on  $V_2O_5$  gels and to Dr. Patricia Goodson (UW) for able assistance with the crystal structure of diDMcT.

## References

1. Abraham, K. M.; Brummer, S. B. In *Lithium Batteries*; Gabano, J. P., Ed.; Academic Press: New York, 1983; Chap. 14, p. 371-406.

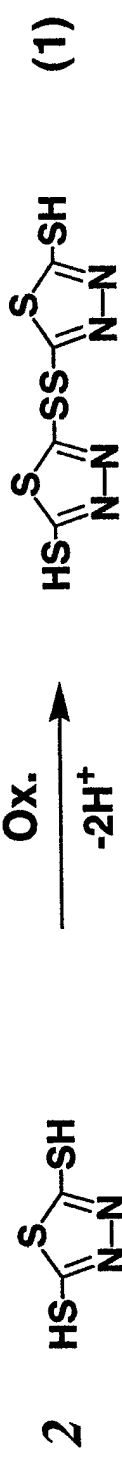
2. Vincent, C. A.; Bonino, F.; Lazzari, M.; Scrosati, B. *Modern Batteries*, Edward Arnold: Maryland, 1984.
3. Brummer, S. B. In *Lithium Battery Technology*, Venkatesetty, H. V., Ed.; Wiley: New York, 1984; Chap. 7, p. 159-177.
4. For a collection of recent contributions in this area, see Megahed, S.; Barnett, B. M.; Xie, L., Eds.; *Rechargeable Lithium and Lithium Ion Batteries*, Electrochemical Society: New Jersey, 1995; Electrochemical Society Proceedings Series PV 94-28.
5. Osaka, T.; Naoi, K.; Hirabayashi, T. *J. Electrochem. Soc.* **1987**, *134*, 2645-2649.
6. Doeff, M. M.; Richardson, T. J.; Kepley, L. *J. Electrochem. Soc.* **1996**, *143*, 2507-2516.
7. Guyomard, D.; Tarascon, J. M. *J. Electrochem. Soc.* **1992**, *139*, 937-948.
8. Ugaji, M.; Hibino, M.; Kudo, T. *J. Electrochem. Soc.* **1995**, *142*, 3664-3668.
9. Le, D. B.; Passerini, S.; Tipton, A. L.; Owens, B. B.; Smyrl, W. H. *J. Electrochem. Soc.* **1995**, *142*, L102-L103.
10. Park, H.-K.; Smyrl, W. H.; Ward, M. D. *J. Electrochem. Soc.* **1995**, *142*, 1068-1073.
11. Le, D. B.; Passerini, S.; Guo, J.; Ressler, J.; Owens, B. B.; Smyrl, W. H. *J. Electrochem. Soc.* **1996**, *143*, 2099-2104.
12. Ein-Eli, Y.; Howard, W. F.; Lu, S. H.; Mukerjee, S.; McBreen, J.; Vaughey, J. T.; Thackeray, M. M. *J. Electrochem. Soc.* **1998**, *145*, 1238-1244.
13. Harreld, J. H.; Dong, W.; Dunn, B. *Mater. Res. Bull. (in press)* **1998**.
14. Whittingham, M. S.; Jacobson, A. J. *Intercalation Chemistry*, Academic Press: New York, 1982.
15. Gamble, F. R.; Disalvo, F. J.; Klemm, R. A.; Geballe, T. H. *Science* **1970**, *168*, 568.
16. Murphy, D. W.; Hull, G. W. *J. Chem. Phys.* **1975**, *62*, 973.
17. Lerf, A.; Schöllhorn, R. *Inorg. Chem.* **1977**, *11*, 2950.
18. Bissessur, R.; DeGroot, D. C.; Schindler, J. L.; Kannewurf, C. R.; Kanatzidis, M. G. *J. Chem. Soc., Chem. Commun.* **1993**, 687-689.
19. Kanatzidis, M. G.; Bissessur, R.; DeGroot, D. C.; Schindler, J. L.; Kannewurf, C. R. *Chem. Mater.* **1993**, *5*, 595-596.
20. Kanatzidis, M. G.; Wu, C. G. *J. Am. Chem. Soc.* **1989**, *111*, 4139-4141.

21. Kanatzidis, M. G.; Tonge, L. M.; Marks, T. J. *J. Am. Chem. Soc.* **1987**, *109*, 3797-3799.
22. Liu, Y.-J.; DeGroot, D. C.; Schindler, J. L.; Kannewurf, C. R.; Kanatzidis, M. G. *J. Chem. Soc., Chem. Commun.* **1993**, 593-596.
23. Kanatzidis, M. G.; Wu, C.-G.; Marcy, H. O.; DeGroot, D. C.; Kannewurf, C. R. *Chem. Mater.* **1990**, *2*, 222-224.
24. Liu, Y.-J.; DeGroot, D. C.; Schindler, J. L.; Kannewurf, C. R.; Kanatzidis, M. G. *Chem. Mater.* **1991**, *3*, 992-994.
25. Lemmon, J. P.; Lerner, M. M. *Chem. Mater.* **1994**, *6*, 207-210.
26. Oriakhi, C. O.; Lerner, M. M. *Chem. Mater.* **1996**, *8*, 2016-2022.
27. Wu, J.; Lerner, M. M. *Chem. Mater.* **1993**, *5*, 835-838.
28. Liu, M.; Visco, S. J.; De Jonghe, L. C. *J. Electrochem. Soc.* **1991**, *138*, 1891.
29. Doeff, M. M.; Lerner, M. M.; Visco, S. J.; De Jonghe, L. C. *J. Electrochem. Soc.* **1992**, *139*, 2077-2081.
30. Sotomura, T.; Uemachi, H.; Miyamoto, Y.; Kaminaga, A.; Oyama, N. *Denki Kagaku* **1993**, *61*, 1366.
31. Oyama, N.; Tatsuma, T.; Sato, T.; Sotomura, T. *Nature* **1995**, *373*, 598.
32. Kaminaga, A.; Tatsuma, T.; Sotomura, T.; Oyama, N. *J. Electrochem. Soc.* **1995**, *142*, L47.
33. Tatsuma, T.; Matsui, H.; Shouji, E.; Oyama, N. *J. Phys. Chem.* **1996**, *100*, 14016.
34. Shouji, E.; Matsui, H.; Oyama, N. *J. Electroanal. Chem.* **1996**, *417*, 17.
35. Shouji, E.; Oyama, N. *J. Electroanal. Chem.* **1996**, *410*, 229.
36. Tatsuma, T.; Sotomura, T.; Sato, T.; Buttry, D. A.; Oyama, N. *J. Electrochem. Soc.* **1995**, *142*, L182.
37. Shouji, E.; Yokoyama, Y.; Pope, J. M.; Oyama, N.; Buttry, D. A. *J. Phys. Chem. B* **1997**, *101*, 2861-2866.
38. Tatsuma, T.; Yokoyama, Y.; Buttry, D. A.; Oyama, N. *J. Phys. Chem. B* **1997**, *101*, 7556-7562.
39. Shouji, E.; Buttry, D. A. *J. Phys. Chem. B* **1998**, *102*, 1444-1449.
40. Aldebert, P.; Baffier, N.; Gharbi, N.; Livage, J. *Mat. Res. Bull.* **1981**, *16*, 669.
41. Legendre, J.; Livage, J. *J. Colloid Interface Sci.* **1983**, *94*, 75.

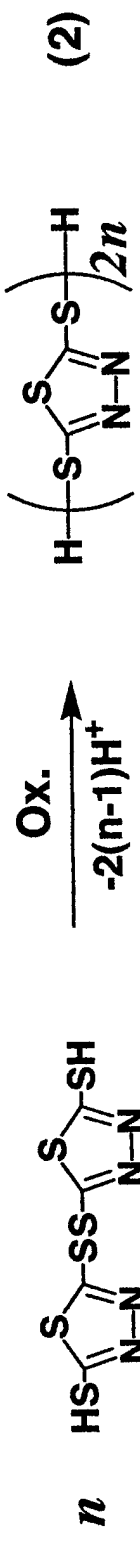
42. Livage, J. *Chem. Mater.* **1991**, *3*, 578.
43. *CRC Handbook of Chemistry and Physics*, CRC Press: Ohio, 1976, 57<sup>th</sup> edition, p. B-174.
44. Pope, J. M.; Buttry, D. A., manuscript in preparation.
45. Pope, J. M.; Oyama, N. *J. Electrochem. Soc.* **1998**, *145*, 1893-1901.

### Figure captions

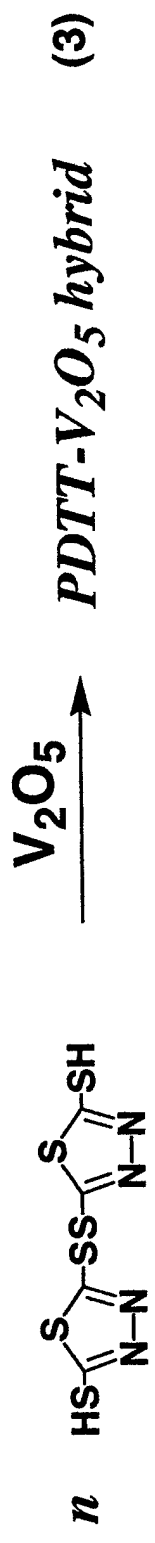
1. a) *In situ* spectroelectrochemical experiment on a V<sub>2</sub>O<sub>5</sub> thin film on ITO. The indicated potentials were applied until the spectral changes were complete, typically ca. 5 min. b) Curve a: *ex situ* spectrum of a V<sub>2</sub>O<sub>5</sub> thin film on ITO. Curve b: *ex situ* spectrum of the same film as in Curve a, after exposure to diDMcT as described in the Experimental section.
2. FTIR spectra of pressed KBr pellets of: a) DMcT, b) PDDT, c) V<sub>2</sub>O<sub>5</sub>, and d) PDTT-V<sub>2</sub>O<sub>5</sub> (see text for details).
3. Cyclic voltammograms of: a) a V<sub>2</sub>O<sub>5</sub> thin film on Au, and b) a PDTT-V<sub>2</sub>O<sub>5</sub> thin film on Au (first scan - solid, second scan - dashed), scan rates = 5 mV s<sup>-1</sup>.
4. Cyclic voltammogram of 5 mM diDMcT, scan rate = 50 mV s<sup>-1</sup>. Steady state response, achieved after multiple scans.
5. Cyclic voltammograms of: a) 10 mM DMcT (repetitive cycles with increasingly positive potential limit), and b) 10 mM DMcT + 2 mM TFMSA (repetitive cycles with increasingly positive potential limit); scan rates = 200 mV s<sup>-1</sup>.



*DMcT Dimer*



*PDTT*





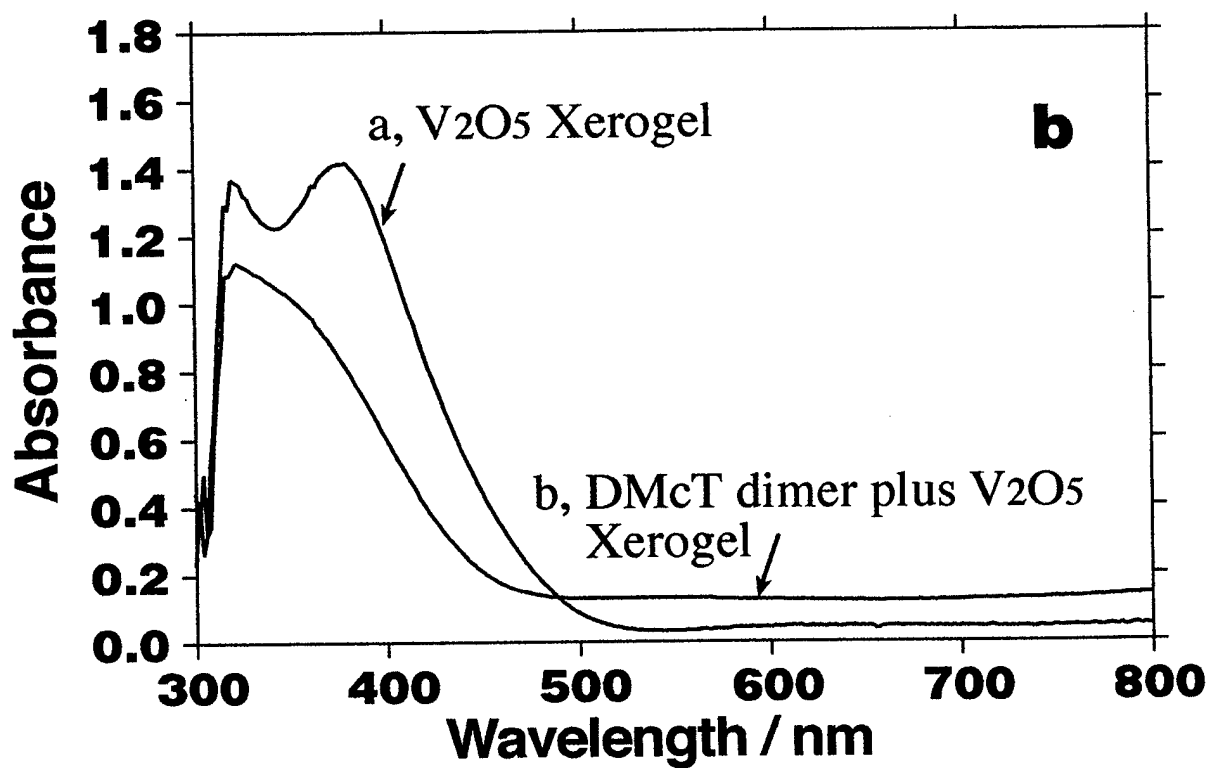
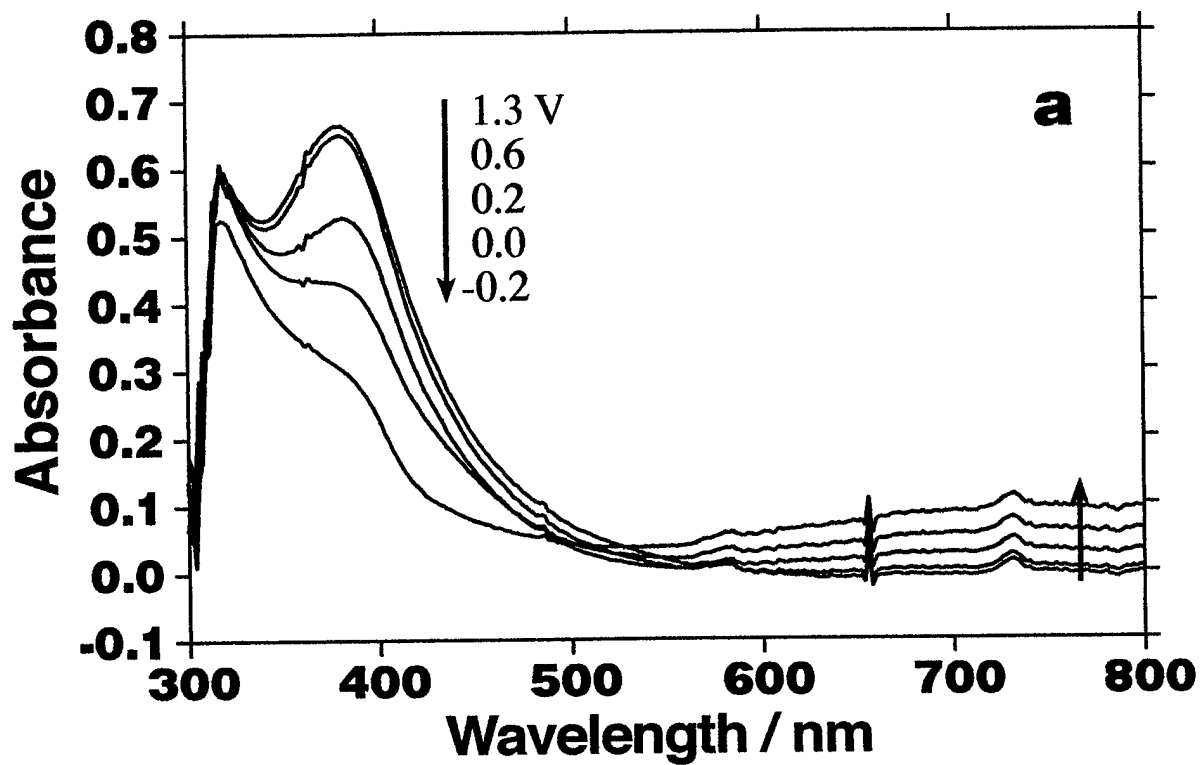


Figure 1

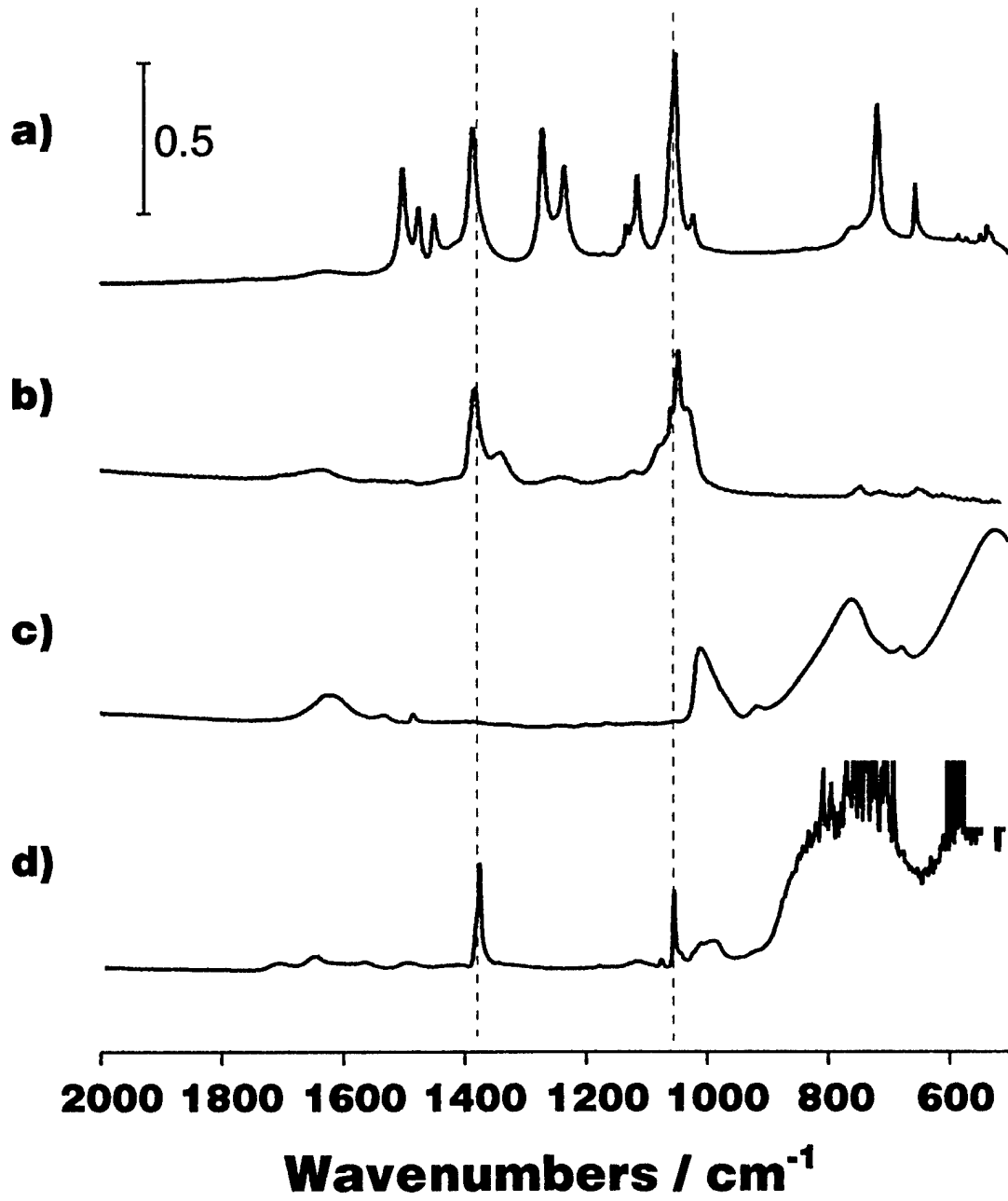


Figure 2

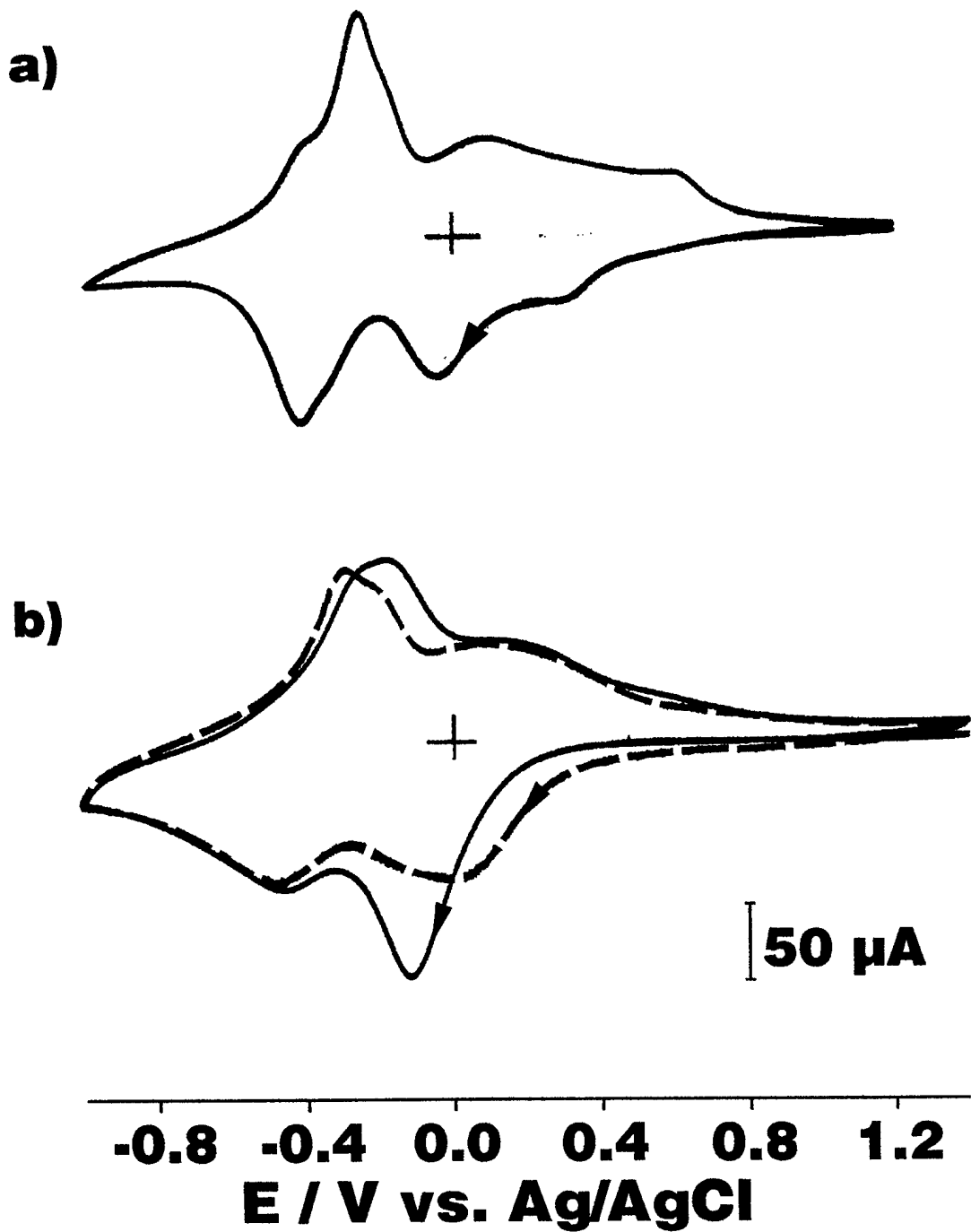


Figure 3

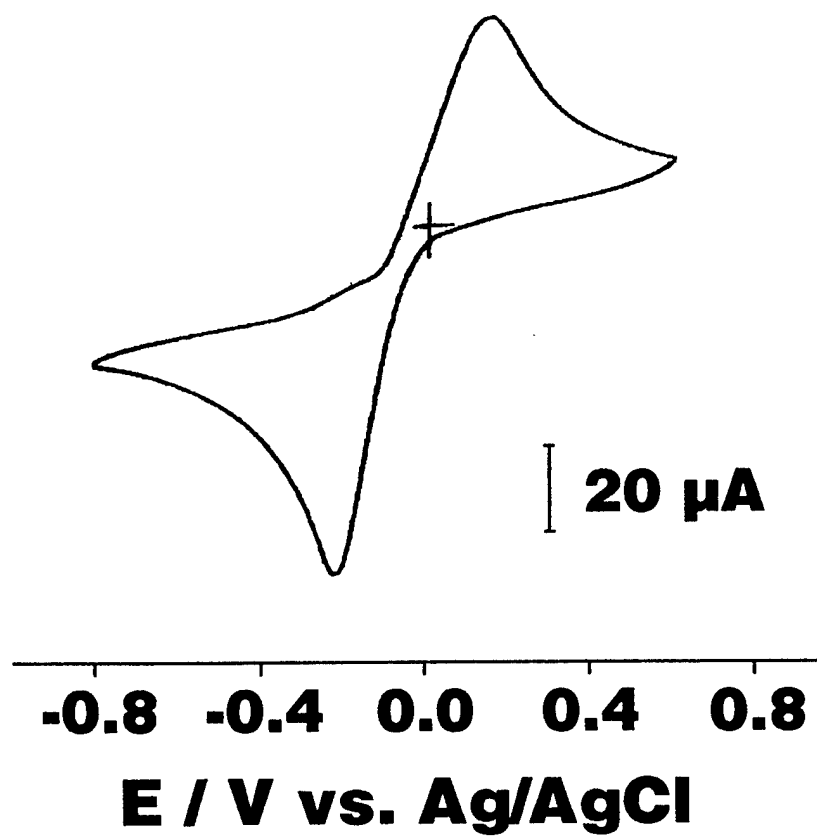


Figure 4

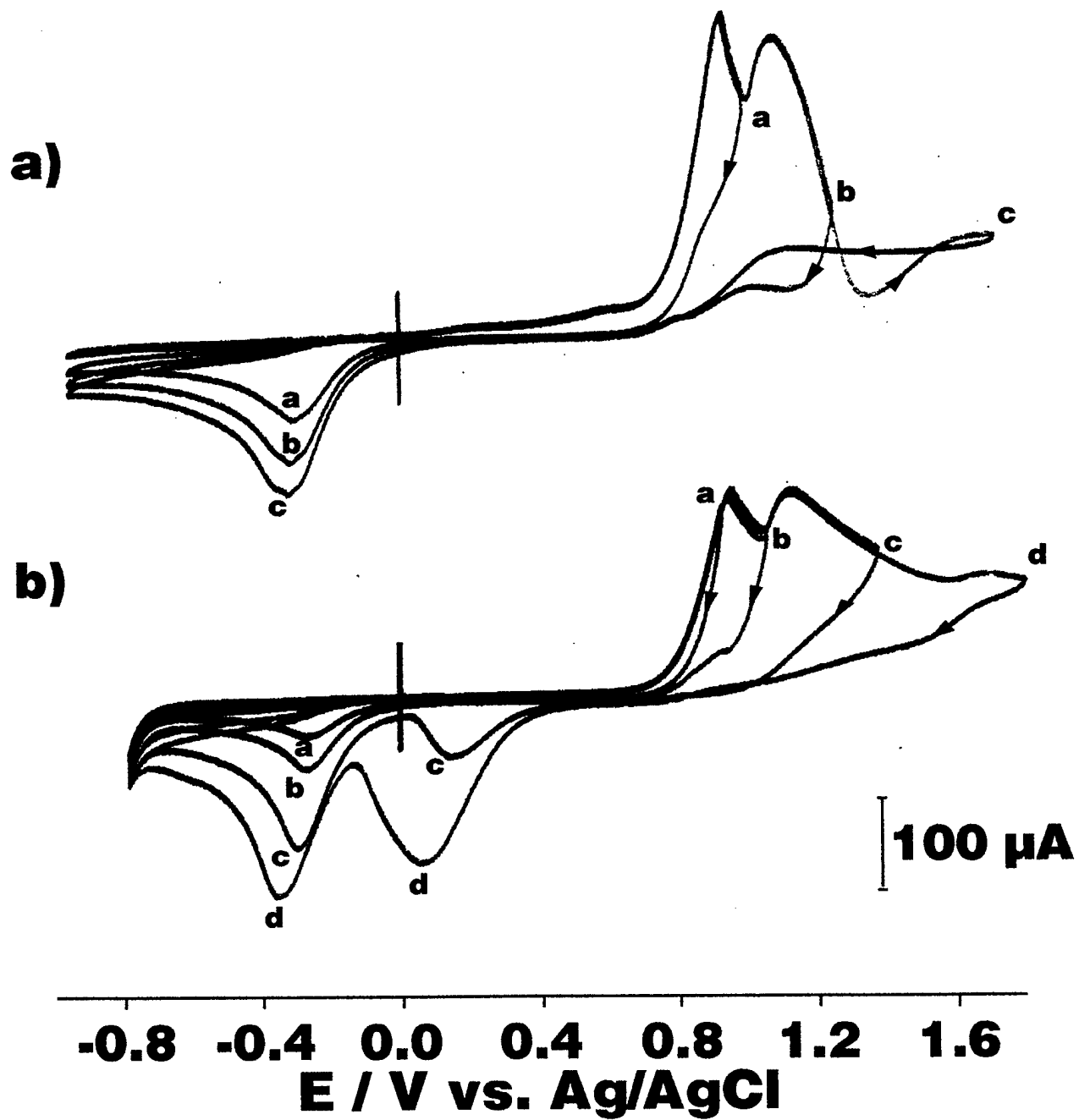


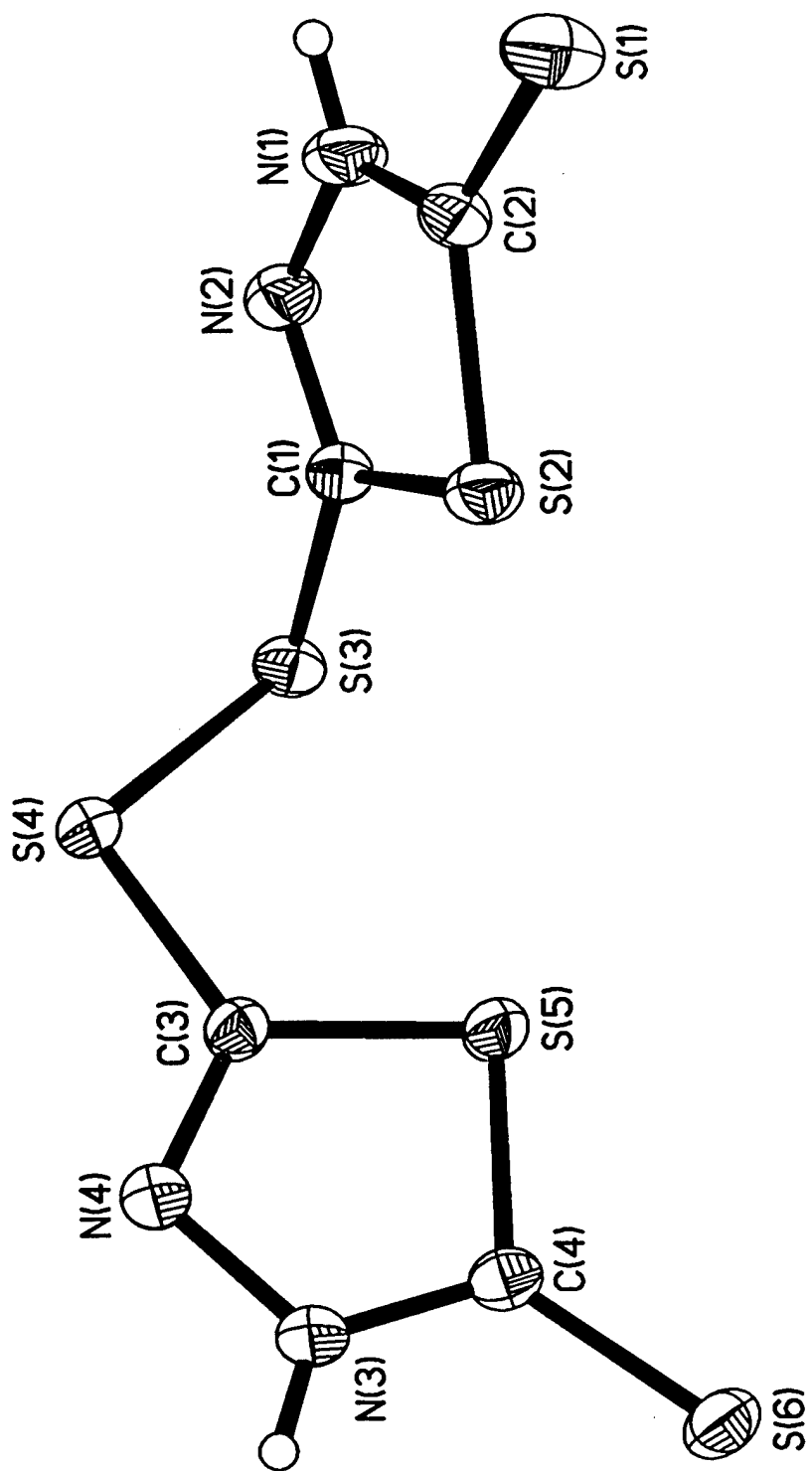
Figure 5

# Supporting Material

Single crystal X-ray data were collected at 25 °C using a yellow crystalline plate of dimensions 0.27 x 0.22 x 0.06 mm on a Siemens P4 diffractometer equipped with a molybdenum tube ( $\lambda = 0.71073 \text{ \AA}$ ) and a graphite monochromator. A cell of dimensions  $a = 5.7200(10) \text{ \AA}$ ,  $b = 5.9170(10) \text{ \AA}$ ,  $c = 15.889(2) \text{ \AA}$ ,  $\alpha = 94.410(10)^\circ$ ,  $\beta = 98.440(10)^\circ$ ,  $\gamma = 104.460(10)^\circ$ , and  $V = 511.46(14) \text{ \AA}^3$  was determined using the measured positions of 41 reflections in the  $2\theta$  range 11 to  $35^\circ$ . A total of 2370 reflections were gathered, the octants collected being  $+h, \pm k, \pm l$ , using omega scans in the  $2\theta$  range 5.2 to  $50^\circ$ . Three standard reflections measured after every 97 reflections collected exhibited less than 4% loss in intensity. The data were integrated and averaged to yield 1788 independent reflections ( $R_{\text{int}} = 0.0233$ ).

The structure was solved by direct methods and refined by full-matrix least-squares techniques on  $F^2$  using structure solution programs from the SHELXTL system.<sup>1</sup> The compound crystallized in the centrosymmetric triclinic space group  $P\bar{1}$  ( $Z = 2$ ). The nonhydrogen atoms were refined anisotropically. Hydrogen atoms were located in the Fourier map and were refined isotropically. The final R factor values were  $R_1 = 0.0308$  and  $wR_2 = 0.0737$  for 1513 data with  $F > 4\sigma F$ . ( $R_1 = 0.0417$  and  $wR_2 = 0.0792$  for all 1788 data giving a data to parameter ratio of 13:1 and a goodness of fit on  $F^2$  of 1.069). The maximum and minimum residual densities remaining were  $0.33 \text{ e\AA}^{-3}$  and  $-0.30 \text{ e\AA}^{-3}$ , respectively. An absorption correction was not applied.

*Reference:* Sheldrick, G. M.; *SHELXTL Crystallographic System*, Version 5.03/Iris (1995), Siemens Analytical X-ray Insts. Inc., Madison, WI.



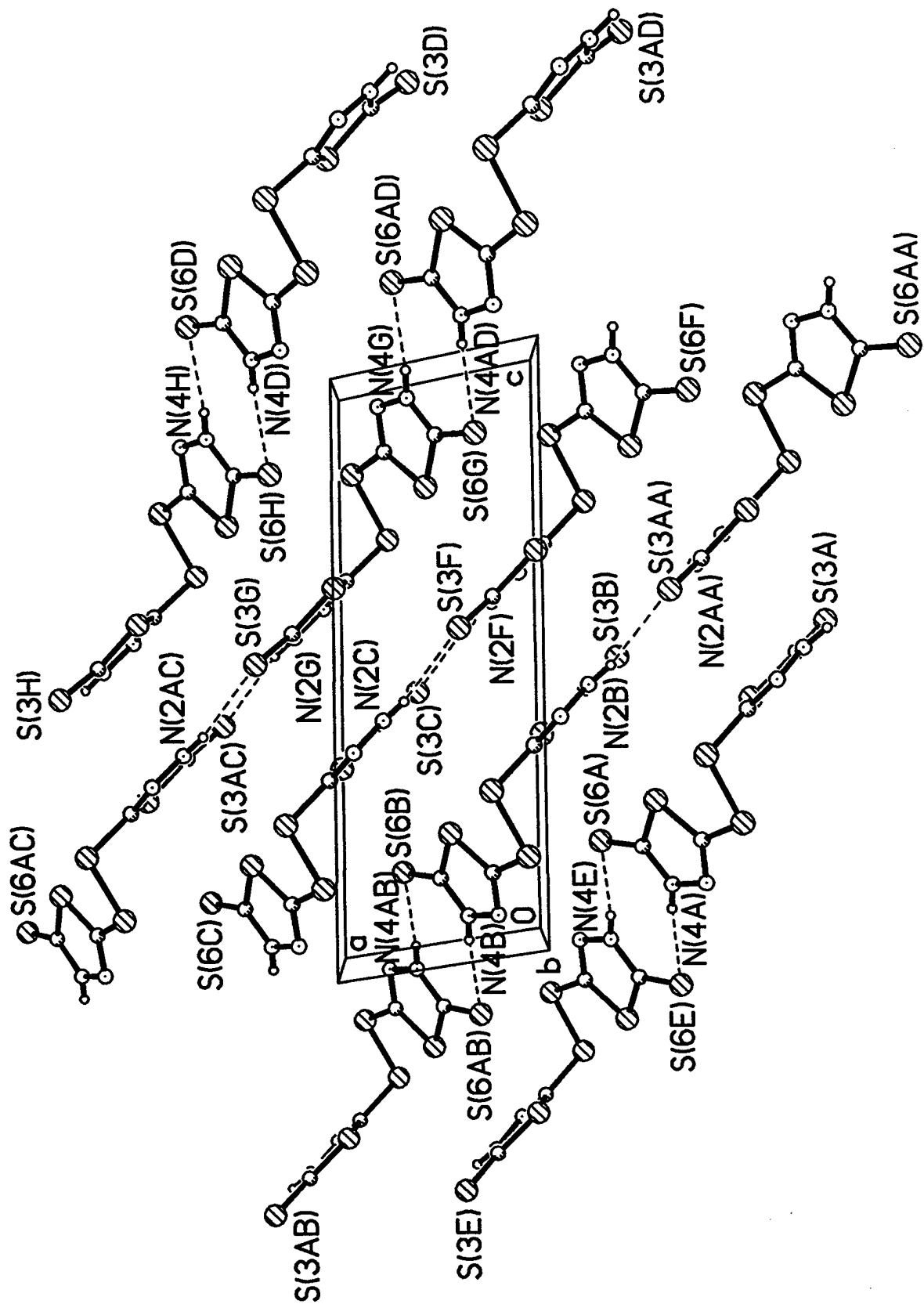


Table 1. Crystal data and structure refinement for 1.

Identification code	pag105b
Empirical formula	$C_4H_2N_4S_6$
Formula weight	298.46
Temperature	293(2) K
Wavelength	0.71073 Å
Crystal system	Triclinic
Space group	$P\bar{1}$
Unit cell dimensions	$a = 5.7200(10)$ Å $\alpha = 94.410(10)^\circ$ $b = 5.9170(10)$ Å $\beta = 98.440(10)^\circ$ $c = 15.889(2)$ Å $\gamma = 104.460(10)^\circ$
Volume, Z	$511.46(14)$ Å <sup>3</sup> , 2
Density (calculated)	$1.938$ Mg/m <sup>3</sup>
Absorption coefficient	$1.297$ mm <sup>-1</sup>
F(000)	300
Crystal size	0.27 x 0.22 x 0.06 mm
$\theta$ range for data collection	2.61 to $25.00^\circ$
Limiting indices	$-1 \leq h \leq 6$ , $-6 \leq k \leq 6$ , $-18 \leq l \leq 18$
Reflections collected	2370
Independent reflections	1788 ( $R_{int} = 0.0233$ )
Refinement method	Full-matrix least-squares on $F^2$
Data / restraints / parameters	1788 / 0 / 135
Goodness-of-fit on $F^2$	1.069
Final R indices [ $I > 2\sigma(I)$ ]	$R1 = 0.0308$ , $wR2 = 0.0737$
R indices (all data)	$R1 = 0.0417$ , $wR2 = 0.0792$
Largest diff. peak and hole	0.325 and $-0.302$ eÅ <sup>-3</sup>

Table 2. Atomic coordinates [ $\times 10^4$ ] and equivalent isotropic displacement parameters [ $\text{\AA}^2 \times 10^3$ ] for 1.  $U(\text{eq})$  is defined as one third of the trace of the orthogonalized  $U_{ij}$  tensor.

	x	y	z	$U(\text{eq})$
S(1)	2500 (1)	8480 (1)	2697 (1)	33 (1)
S(2)	-114 (1)	4012 (1)	3431 (1)	35 (1)
S(3)	-3950 (2)	2145 (1)	4511 (1)	44 (1)
S(4)	762 (1)	7046 (1)	1474 (1)	31 (1)
S(5)	4509 (1)	4253 (1)	2005 (1)	34 (1)
S(6)	6931 (1)	615 (1)	1365 (1)	38 (1)
N(1)	-836 (5)	8097 (4)	3715 (2)	39 (1)
N(2)	-2270 (5)	6576 (5)	4148 (2)	40 (1)
N(3)	2186 (5)	4013 (4)	477 (2)	40 (1)
N(4)	3652 (5)	2501 (4)	486 (2)	37 (1)
C(1)	395 (5)	6988 (5)	3308 (2)	31 (1)
C(2)	-2246 (5)	4296 (5)	4078 (2)	32 (1)
C(3)	2450 (5)	5043 (4)	1243 (2)	27 (1)
C(4)	5028 (5)	2322 (4)	1210 (2)	28 (1)

Table 3. Bond lengths [Å] and angles [°] for 1.

S(1)-C(1)	1.765(3)	S(1)-S(4)	2.0602(10)
S(2)-C(2)	1.737(3)	S(2)-C(1)	1.743(3)
S(3)-C(2)	1.660(3)	S(4)-C(3)	1.755(3)
S(5)-C(3)	1.736(3)	S(5)-C(4)	1.745(3)
S(6)-C(4)	1.666(3)	N(1)-C(1)	1.282(3)
N(1)-N(2)	1.360(4)	N(2)-C(2)	1.349(4)
N(2)-H(1)	0.84(4)	N(3)-C(3)	1.289(3)
N(3)-N(4)	1.370(3)	N(4)-C(4)	1.323(4)
N(4)-H(2)	0.79(3)		
C(1)-S(1)-S(4)	100.87(10)	C(2)-S(2)-C(1)	89.11(13)
C(3)-S(4)-S(1)	101.01(9)	C(3)-S(5)-C(4)	89.10(13)
C(1)-N(1)-N(2)	109.0(2)	C(2)-N(2)-N(1)	119.5(2)
C(2)-N(2)-H(1)	118(3)	N(1)-N(2)-H(1)	122(3)
C(3)-N(3)-N(4)	108.5(2)	C(4)-N(4)-N(3)	120.0(2)
C(4)-N(4)-H(2)	123(3)	N(3)-N(4)-H(2)	117(3)
N(1)-C(1)-S(2)	115.4(2)	N(1)-C(1)-S(1)	120.5(2)
S(2)-C(1)-S(1)	124.1(2)	N(2)-C(2)-S(3)	127.0(2)
N(2)-C(2)-S(2)	106.9(2)	S(3)-C(2)-S(2)	126.1(2)
N(3)-C(3)-S(5)	115.3(2)	N(3)-C(3)-S(4)	120.9(2)
S(5)-C(3)-S(4)	123.8(2)	N(4)-C(4)-S(6)	127.9(2)
N(4)-C(4)-S(5)	107.1(2)	S(6)-C(4)-S(5)	125.0(2)

Symmetry transformations used to generate equivalent atoms:

Table 4. Anisotropic displacement parameters [ $\text{\AA}^2 \times 10^3$ ] for 1.

The anisotropic displacement factor exponent takes the form:

$$-2\pi^2 [ (ha^*)^2 U_{11} + \dots + 2hka^* b^* U_{12} ]$$

	U11	U22	U33	U23	U13	U12
S(1)	38(1)	31(1)	31(1)	-1(1)	9(1)	9(1)
S(2)	43(1)	34(1)	32(1)	3(1)	15(1)	17(1)
S(3)	53(1)	42(1)	42(1)	4(1)	23(1)	13(1)
S(4)	32(1)	35(1)	30(1)	2(1)	6(1)	16(1)
S(5)	37(1)	39(1)	29(1)	-4(1)	1(1)	20(1)
S(6)	38(1)	38(1)	41(1)	-4(1)	2(1)	20(1)
N(1)	48(2)	39(1)	38(1)	5(1)	15(1)	22(1)
N(2)	49(2)	43(2)	38(1)	4(1)	20(1)	22(1)
N(3)	50(2)	48(2)	30(1)	1(1)	6(1)	30(1)
N(4)	48(2)	41(1)	27(1)	-2(1)	6(1)	24(1)
C(1)	35(2)	35(2)	26(1)	0(1)	6(1)	14(1)
C(2)	35(2)	41(2)	22(1)	0(1)	5(1)	13(1)
C(3)	28(1)	26(1)	30(1)	4(1)	7(1)	9(1)
C(4)	27(1)	25(1)	32(1)	-1(1)	8(1)	4(1)

Table 5. Hydrogen coordinates ( $\times 10^4$ ) and isotropic displacement parameters ( $\text{\AA}^2 \times 10^3$ ) for 1.

	x	y	z	U(eq)
H(1)	-3310(71)	6967(68)	4409(25)	72(13)
H(2)	3631(63)	1777(58)	47(22)	50(10)

Table 6. Observed and calculated structure factors for 1

h k l 10Fo 10Fc 10s						h k l 10Fo 10Fc 10s						h k l 10Fo 10Fc 10s						h k l 10Fo 10Fc 10s											
1	0	0	13	6	6	0	-4	1	65	65	2	1	3	1	83	81	2	1	-1	2	411	423	4	-2	-5	3	85	83	4
2	0	0	36	43	4	0	-4	1	151	141	4	2	3	1	405	407	7	2	-1	2	352	329	4	-1	-5	3	37	29	9
3	0	0	227	226	4	2	-4	1	300	311	7	3	3	1	237	237	5	3	-1	2	430	425	5	0	0	0	151	148	2
4	0	0	236	241	4	3	-4	1	24	11	15	4	3	1	131	130	5	4	-1	2	225	218	4	0	-5	3	410	410	5
5	0	0	0	7	1	4	-4	1	36	45	9	5	3	1	0	24	1	5	-1	2	137	136	3	2	-5	3	44	58	7
6	0	0	113	109	3	5	-4	1	155	150	4	-6	4	1	37	37	10	-6	0	2	68	69	5	5	-5	3	222	227	4
7	0	0	57	42	6	6	-4	1	0	4	4	-5	4	1	23	18	23	-6	0	2	121	125	3	4	-5	3	84	89	4
8	0	0	259	267	5	5	-3	1	125	121	3	-4	4	1	174	175	4	-5	0	2	252	246	5	5	-5	3	0	10	10
9	0	0	342	342	7	7	-3	1	40	34	8	-3	4	1	28	21	11	-4	0	2	341	335	7	-4	-4	3	111	112	3
10	0	0	68	63	2	2	-3	1	313	323	5	-2	4	1	554	573	6	-3	0	2	349	356	6	-3	-4	3	133	132	3
11	0	0	413	414	4	4	-3	1	62	65	4	-1	4	1	156	161	2	-2	0	2	44	43	3	-2	-4	3	50	51	6
12	0	0	533	552	5	5	-3	1	0	12	1	0	4	1	248	247	3	-1	0	2	193	188	2	-1	-4	3	146	143	2
13	0	0	412	415	2	2	-3	1	553	546	3	1	4	1	353	359	5	0	0	2	229	241	2	0	-4	3	359	345	5
14	0	0	80	72	1	1	-3	1	257	252	6	2	4	1	131	127	3	2	0	2	605	602	9	1	-4	3	168	172	3
15	0	0	320	308	2	2	-3	1	387	403	6	3	4	1	53	41	6	1	0	2	362	339	4	2	-4	3	0	9	1
16	0	0	184	185	3	3	-3	1	148	143	3	4	4	1	33	20	12	3	0	2	278	290	6	3	-4	3	73	74	4
17	0	0	24	37	16	1	-3	1	128	135	3	-5	5	1	0	5	1	4	0	2	123	122	2	4	-4	3	64	66	4
18	0	0	0	0	24	1	-3	1	89	95	4	-4	5	1	318	322	6	5	0	2	66	71	5	5	-4	3	109	104	3
19	0	0	46	58	9	6	-3	1	81	66	4	-3	5	1	161	170	3	6	0	2	43	45	8	-6	-6	3	0	10	4
20	0	0	219	217	4	4	-2	1	49	39	7	-2	5	1	128	125	2	-6	1	2	43	51	8	-5	-3	3	147	153	1
21	0	0	78	74	4	4	-2	1	313	324	5	-1	5	1	18	17	17	-5	1	2	41	37	7	-4	-3	3	33	31	11
22	0	0	397	394	4	4	-2	1	72	69	6	0	1	1	428	428	15	-4	1	2	80	78	3	-3	-3	3	273	275	5
23	0	0	240	239	7	7	-2	1	267	255	6	0	5	1	53	56	4	-3	1	2	55	38	3	-2	-3	3	95	97	2
24	0	0	155	169	3	3	-2	1	231	229	3	2	5	1	128	129	3	-2	1	2	942	984	4	-1	-3	3	310	314	4
25	0	0	523	548	3	3	-2	1	118	117	2	3	5	1	38	43	10	-1	1	2	118	113	2	0	0	3	45	47	3
26	0	0	292	286	5	5	-2	1	127	122	2	-4	6	1	62	61	6	0	1	2	89	85	1	1	-1	3	34	20	5
27	0	0	322	312	6	6	-2	1	153	148	3	-3	6	1	109	108	3	1	1	2	419	410	3	2	-3	3	151	147	7
28	0	0	454	450	6	6	-2	1	132	128	3	-2	6	1	75	69	4	2	1	2	311	304	5	3	-3	3	301	311	7
29	0	0	187	187	3	3	-4	1	13	14	13	-1	6	1	97	96	2	3	1	2	183	180	3	4	-3	3	224	224	4
30	0	0	15	4	14	1	-4	1	107	107	3	0	6	1	193	195	2	4	1	2	177	177	3	5	-5	3	115	115	3
31	0	0	46	45	8	8	-6	1	70	68	6	0	6	1	82	83	3	5	1	2	104	100	3	6	-6	3	0	10	1
32	0	0	59	65	6	6	-1	1	201	201	5	-1	-6	2	83	78	4	-6	2	2	66	69	6	-5	-2	3	12	3	12
33	0	0	58	66	5	5	-5	1	56	62	6	0	0	1	32	28	21	-5	2	2	154	152	4	-4	-2	3	49	43	6
34	0	0	258	261	5	5	-4	1	161	164	6	-4	-6	2	53	57	5	-4	2	2	176	179	3	-3	-2	3	136	133	3
35	0	0	397	422	6	6	-3	1	57	56	5	2	-6	2	67	65	5	-4	2	2	263	264	4	-2	-2	3	203	207	4
36	0	0	167	171	3	3	-2	1	624	600	3	-2	-6	2	25	6	19	-3	2	2	611	627	5	-1	-2	3	66	59	1
37	0	0	200	198	2	2	-1	1	602	581	5	-4	-6	2	130	129	3	-2	2	2	251	251	5	0	0	3	333	337	6
38	0	0	63	68	3	3	0	1	36	34	1	-2	-5	2	0	8	1	-1	1	2	125	133	4	1	-2	3	52	50	4
39	0	0	271	265	3	3	-1	1	90	88	1	-2	-5	2	101	101	3	0	0	2	512	514	3	2	-2	3	133	132	2
40	0	0	137	128	3	3	-1	1	404	385	4	-1	-5	2	42	41	5	2	2	2	96	46	2	3	-2	3	172	168	3
41	0	0	147	148	5	5	-4	1	445	436	3	0	-5	2	75	72	3	2	2	2	98	95	2	4	-2	3	71	68	4
42	0	0	62	62	5	5	-1	1	85	86	3	1	-5	2	276	271	6	3	3	2	0	19	1	5	-2	3	0	2	1
43	0	0	81	79	4	4	-1	1	53	61	6	2	-5	2	101	101	3	4	4	2	169	171	3	6	-6	3	197	191	4
44	0	0	115	110	3	3	-6	1	170	169	4	5	-5	2	86	91	3	5	2	2	105	99	3	-6	-1	3	117	120	3
45	0	0	158	157	4	4	0	1	7	11	7	5	-5	2	58	63	5	-6	3	2	162	161	4	-5	-1	3	61	63	5
46	0	0	393	393	8	8	-5	1	0	0	1	-4	-4	2	204	206	4	-4	4	2	131	136	3	-4	-1	3	209	208	4
47	0	0	201	214	4	4	-4	0	85	88	1	-3	-4	2	101	94	4	-5	4	2	319	333	5	-3	-1	3	220	216	4
48	0	0	22	17	21	2	-3	0	0	9	5	-2	-4	2	41	39	8	-3	3	2	197	192	4	-2	-1	3	113	107	7
49	0	0	198	193	2	2	-2	0	29	22	1	-1	-4	2	45	58	6	-1	-1	2	116	113	3	-1	-1	3	996	978	2
50	0	0	42	50	10	1	-1	0	34	31	1	-1	-4	2	59	65	3	-1	-4	2	243	246	3	0	-1	3	274	257	2
51	0	0	73	75	3	3	0	0	404	398	2	0	-4	2	256	253	2	0	0	2	86	91	1	1	-1	3	32	31	3
52	0	0	98	94	3	3	2	1	239	226	5	1	-4	2	147	146	2	3	3	2	136	140	2	2	-1	3	129	124	2
53	0	0	99	103	3	3	4	0	139	137	2	2	-4	2	222	228	4	2	3	2	146	149	4	3	-1	3	134	135	2
54	0	0	31	17	13	5	4	0	96	95	3	3	-4	2	424	462	7	4	4	2	16	8	16	4	-4	3	246	249	4
55	0	0	257	254	5	5	0	0	398	387	8	4	-4	2	37	11	8	4	4	3	117	120	3	5	-1	3	30	18	11
56	0	0	58	51	7	7	-6	0	18	23	18	5	-4	2	167	170	4	-6	4	2	190	181	3	6	0	3	83	80	4
57	0	0	7	3	5	5	-6	1	106	97	3	6	-4	2	63	62	6	-5	4	2	0	16	1	-6	0	3	109	113	3
58	0	0	134	137	2	2	-5	1	156	154	3	-5	-3	2	47	34	7	-4	4	2	62	64	4	-5	0	3	76	65	4
59	0	0	136	132	2	2	-3	1	94	95	5	-4	-3	2	25	11	19	-3	4	2	109	104	2	-4	0	3	247	237	4
60	0	0	128	126	2	2	-3	1	36	34	5	-3	-3	2	0	12	1	-2	4	2	36	39	7	-3	0	3	189	186	3
61	0	0	74	79	4	4	-2	1	435	442																			

Table 6. Observed and calculated structure factors for 1

10Fo						10Fc						10s						10Fo						10Fc						10s					
h	k	l	10Fo	10Fc	10s	h	k	l	10Fo	10Fc	10s	h	k	l	10Fo	10Fc	10s	h	k	l	10Fo	10Fc	10s	h	k	l	10Fo	10Fc	10s	h	k	l	10Fo	10Fc	10s
1	2	3	212	215	2	6	-2	4	83	76	4	1	-6	5	43	38	5	-2	2	5	186	199	3	5	-2	6	63	57	5						
2	2	3	397	394	6	-6	-1	4	54	59	6	2	-6	5	82	84	4	-1	2	5	53	56	2	5	-2	6	173	173	3						
3	2	3	67	69	4	-5	-1	4	121	127	3	3	-6	5	37	20	9	0	2	5	253	243	4	4	-6	-1	6	34	11	11					
4	2	3	41	45	8	-4	-1	4	0	29	1	4	-6	5	16	1	15	1	2	2	354	358	6	6	-5	-1	6	111	107	3					
5	2	3	21	29	20	-3	-1	4	36	25	6	-3	-5	5	65	59	5	2	2	2	142	140	3	3	-4	-1	6	318	317	5					
6	2	3	53	49	6	-2	-1	4	214	206	4	-2	-5	5	151	142	4	-4	2	2	118	122	3	3	-3	-1	6	0	16	1					
7	2	3	164	155	4	-1	-1	4	712	695	3	-1	-5	5	36	36	6	4	2	5	75	76	4	4	-2	-1	6	189	173	3					
8	2	3	36	26	7	0	-1	4	83	86	7	0	-5	5	160	157	4	5	2	5	63	72	6	6	-1	-1	6	135	131	1					
9	2	3	327	336	6	1	-1	4	524	527	7	1	-5	5	118	114	2	-6	3	5	160	158	4	4	0	-1	6	49	38	4					
10	2	3	301	316	6	2	-1	4	226	226	4	2	-5	5	292	295	5	-5	3	5	0	2	1	1	-1	-1	6	47	53	3					
11	2	3	300	299	4	3	-1	4	15	27	15	3	-5	5	36	19	8	-4	3	5	92	98	3	3	2	-1	6	401	386	6					
12	2	3	58	59	3	4	-1	4	248	245	5	4	-5	5	90	89	4	-3	3	5	327	348	7	7	3	-1	6	137	134	3					
13	2	3	385	381	9	5	-1	4	29	14	12	5	-5	5	57	50	6	-2	3	5	403	412	6	6	4	-1	6	285	289	5					
14	2	3	216	218	4	6	-1	4	33	35	12	-4	-4	5	0	15	1	-1	3	5	85	90	2	2	5	-1	6	34	26	10					
15	2	3	101	97	3	-6	0	4	40	41	9	-3	-4	5	72	76	4	0	3	5	500	502	4	4	-6	0	6	11	13	11					
16	2	3	69	66	4	-5	0	4	54	55	5	-2	-4	5	30	39	11	1	1	3	51	56	3	3	-5	0	6	159	156	3					
17	2	3	171	167	3	-4	0	4	92	88	3	-1	-4	5	133	135	2	-2	3	5	201	195	4	4	-4	0	6	188	179	3					
18	2	3	274	264	5	-3	0	4	424	422	5	0	-4	5	36	25	5	3	3	3	119	121	3	3	-3	0	6	382	381	6					
19	2	3	57	53	5	-2	0	4	450	436	4	1	-4	5	462	469	4	-4	4	3	103	110	4	4	-2	0	6	49	59	3					
20	2	3	156	158	2	-1	0	4	30	22	3	2	-4	5	234	232	4	-6	4	5	61	53	6	6	-1	0	6	506	508	5					
21	2	3	131	132	3	0	0	4	582	601	2	3	-4	5	58	55	4	-5	4	5	213	216	4	4	0	0	6	170	170	2					
22	2	3	202	206	3	1	0	4	902	910	11	4	-4	5	198	200	4	-4	4	5	38	30	8	8	1	0	6	176	170	2					
23	2	3	97	97	2	2	0	4	21	7	10	5	-4	5	61	52	5	-3	4	5	49	44	6	6	2	0	6	879	888	5					
24	2	3	255	259	7	3	0	4	71	59	3	-5	-3	5	117	115	3	-2	4	4	217	220	4	4	3	0	6	58	56	4					
25	2	3	107	102	3	4	0	4	54	44	5	-4	-3	5	52	42	6	-1	4	5	327	329	5	5	4	0	6	102	105	3					
26	2	3	0	7	1	5	0	4	174	176	3	-3	-3	5	272	265	5	0	4	5	55	50	3	3	5	0	6	41	17	8					
27	2	3	149	142	4	6	0	4	122	116	3	-2	-3	5	332	320	7	1	4	4	22	20	12	12	-6	1	6	31	36	12					
28	2	3	283	289	5	-6	1	4	193	185	4	-1	-3	5	267	261	3	2	4	4	145	147	3	3	-5	1	6	161	162	3					
29	2	3	151	149	3	-5	1	4	277	272	5	0	-3	5	444	443	11	-3	4	4	86	84	4	4	-4	1	6	182	178	3					
30	2	3	17	10	17	-4	1	4	238	232	4	0	-3	5	10	8	10	-5	5	5	0	1	1	1	-3	1	6	281	282	6					
31	2	3	330	326	4	-3	1	4	340	339	5	2	-3	5	206	204	4	-4	5	5	109	111	3	3	-2	1	6	439	435	5					
32	2	3	110	104	2	-2	1	4	109	102	2	3	-3	5	262	270	4	-3	5	5	171	170	3	3	-1	1	6	292	294	3					
33	2	3	172	172	5	-1	1	4	23	24	2	4	-3	5	114	115	3	-2	5	5	182	182	4	4	0	1	6	287	284	3					
34	2	3	17	3	16	0	0	4	230	221	3	5	-3	5	212	211	4	-1	5	5	45	42	7	7	1	1	6	350	341	4					
35	2	3	24	25	23	2	1	4	76	73	2	6	-3	5	99	102	4	0	0	5	37	28	7	7	2	1	6	16	19	16					
36	2	3	72	74	5	2	1	4	93	91	2	-5	-2	5	148	149	3	1	5	5	33	27	7	7	3	1	6	140	146	2					
37	2	3	257	255	5	3	1	4	292	302	7	-3	-2	5	0	8	1	2	2	5	46	35	8	8	4	1	6	153	161	3					
38	2	3	48	47	5	5	1	4	0	2	1	-4	-2	5	290	290	5	-4	6	5	21	19	21	21	5	1	6	43	30	8					
39	2	3	42	24	3	5	1	4	36	46	10	-2	-2	5	327	333	6	-3	6	5	96	104	4	4	-6	2	6	46	40	7					
40	2	3	85	81	3	-6	2	4	143	142	3	-1	-2	5	11	2	10	-2	6	5	96	93	4	4	-5	2	6	273	267	5					
41	2	3	39	39	6	-5	2	4	213	216	3	0	-2	5	59	57	2	-1	6	5	136	139	2	2	-4	2	6	238	234	4					
42	2	3	63	62	4	-4	2	4	168	176	3	1	-2	5	129	131	3	0	6	5	0	1	1	1	-3	2	6	95	97	2					
43	2	3	72	64	3	-3	2	4	273	272	6	-2	2	4	507	522	5	-1	-6	6	81	75	3	3	-2	2	6	440	444	5					
44	2	3	110	109	3	-2	2	4	300	315	6	3	-2	5	372	385	7	0	-6	6	268	262	4	4	-1	2	6	30	24	4					
45	2	3	110	109	3	-1	2	4	101	103	2	4	-2	5	0	11	1	1	-6	6	131	132	2	2	0	2	6	469	478	4					
46	2	3	225	223	5	0	2	4	212	217	2	5	-2	5	66	68	5	2	-6	6	32	30	12	12	1	2	6	378	386	8					
47	2	3	95	91	4	1	2	4	558	553	8	6	-2	5	87	81	4	3	-6	6	27	26	17	17	2	2	6	92	91	3					
48	2	3	71	68	4	2	2	4	68	58	3	-6	-1	5	95	102	4	-4	-6	6	44	40	8	8	3	2	6	55	49	5					
49	2	3	87	80	2	3	2	4	139	137	3	-5	-1	5	8	18	7	-3	-5	6	31	19	12	12	4	2	6	86	88	4					
50	2	3	27	26	8	4	2	4	107	101	3	-4	-1	5	235	237	4	-2	-5	6	74	75	4	4	-6	3	6	52	52	6					
51	2	3	180	179	2	5	2	4	89	96	4	-3	-1	5	32	32	7	-1	-5	6	151	151	2	2	-5	3	6	87	87	4					
52	2	3	160	165	4	-6	3	4	82	73	4	0	-1	5	257	255	5	0	-5	6	95	98	2	2	-4	3	6	29	38	11					
53	2	3	83	75	3	-5	3	4	175	173	3	-1	-1	5	300	292	5	-1	-5	6	117	115	2	2	-3	3	6	89	79	3					
54	2	3	0	10	1	-4	3	4	110	113	3	0	-1	5	72	68	1	2	-5	6	222	228	4	4	-2	3	6	54	61	4					
55	2	3	46	36	7	-3	3	4	348	367	6	1	-1	5	262	264	3	3	-5	6	93	91	3	3	-1	3	6	405	403	4					
56	2	3	166	185	5	-2	3	4	87	88	2	-2	-1	5	264	262	5	4	-5	6	5	29	5	5	0	3	6	47	49	4					
57	2	3	67	73	5	-1	3	4	171	180	2	3	-1	5	234	228	4	5	-5	6	37	35	11	11	1	3	6	88	89	2					
58	2	3	23	10	20	0	3	4	218	215	3	4	-1	5	442	433																			

Table 6. Observed and calculated structure factors for 1

h k l			10Fo	10Fc	10s	h k l			10Fo	10Fc	10s	h k l			10Fo	10Fc	10s	h k l			10Fo	10Fc	10s								
-3	-5	7	24	23	23	-5	3	7	92	93	3	-5	0	8	142	141	3	0	-3	9	71	73	6	-2	-6	10	57	53	6		
-2	-5	7	40	26	8	-4	3	7	226	228	4	-4	0	8	225	221	4	1	-3	9	382	386	5	-2	-5	10	62	53	5		
-1	-5	7	124	119	2	-3	3	7	180	179	3	-3	0	8	177	185	3	2	-3	9	317	322	5	-1	-5	10	42	46	5		
0	-5	7	231	226	3	-2	3	7	45	32	5	-2	0	8	110	109	2	3	-3	9	98	96	3	0	-5	10	0	3	1		
1	-5	7	239	243	5	-1	3	7	62	58	2	-1	0	8	386	378	3	4	-3	9	0	0	1	1	-5	10	29	23	8		
2	-5	7	47	62	7	0	3	7	82	83	3	0	0	8	37	36	3	5	-3	9	85	79	4	2	-5	10	11	10	10		
3	-5	7	32	34	11	1	3	7	64	66	3	1	0	8	84	86	1	1	-2	9	199	201	4	3	-5	10	0	22	1		
4	-5	7	86	80	4	2	3	7	117	111	3	2	0	8	278	272	4	1	-2	9	108	106	3	4	-5	10	43	38	9		
4	-4	7	144	144	3	3	3	7	0	8	1	3	0	8	0	9	1	1	-3	9	105	102	3	-3	-4	10	0	20	1		
3	-4	7	35	28	10	4	3	7	176	175	4	4	0	8	0	13	1	1	-2	9	42	45	5	-2	-4	10	136	136	3		
2	-4	7	177	181	4	-6	4	7	16	0	16	5	0	8	157	156	3	1	-2	9	214	215	3	-1	-4	10	85	84	6		
1	-4	7	0	17	1	-5	4	7	143	141	3	-6	1	8	53	46	6	1	0	-2	9	152	151	2	0	-4	10	145	144	2	
0	-4	7	142	141	6	-4	4	7	148	144	3	-5	1	8	0	20	1	1	-2	9	121	125	3	1	-4	10	37	44	6		
0	-4	7	89	89	2	-3	4	7	97	95	3	-4	1	8	24	39	20	2	-2	9	61	61	4	2	-4	10	70	70	4		
1	-4	7	25	1	15	-2	4	7	233	240	4	-3	1	8	145	139	3	3	-2	9	59	57	5	3	-4	10	53	48	6		
2	-4	7	54	42	5	-1	4	7	54	45	6	-2	1	8	0	5	1	1	-2	9	71	68	4	4	-4	10	176	180	3		
3	-4	7	302	301	5	0	4	7	331	334	5	-1	1	8	110	110	2	2	-2	9	35	25	11	-4	-3	10	0	14	1		
4	-4	7	63	69	6	1	4	7	0	7	1	0	0	1	8	635	649	13	3	-1	9	0	22	1	-3	-3	10	58	65	5	
5	-4	7	35	22	11	2	4	7	168	172	4	2	1	8	44	42	6	6	-4	-1	9	255	252	5	-2	-3	10	39	38	7	
5	-4	7	0	0	1	3	4	7	72	76	5	2	1	8	105	106	3	3	-3	-1	9	275	288	5	-1	-3	10	43	36	4	
3	-3	7	210	219	4	-5	5	7	49	31	7	3	1	8	16	22	15	4	-2	-1	9	320	313	6	0	0	10	74	75	2	
2	-3	7	47	52	5	-4	5	7	50	58	7	4	1	8	215	211	4	4	-1	-1	9	377	366	4	1	-3	10	70	77	3	
1	-3	7	426	421	4	-3	5	7	214	212	4	5	1	8	41	40	10	24	0	-1	9	202	197	5	2	-3	10	262	267	5	
0	-3	7	83	86	2	-2	5	7	95	89	3	-6	2	8	24	33	24	4	2	-1	9	45	38	3	3	-3	10	102	99	3	
0	-3	7	102	96	1	-1	5	7	142	143	3	-5	2	8	82	90	4	4	1	-1	9	0	3	1	4	-3	10	22	14	22	
1	-3	7	390	395	7	0	0	5	7	143	142	2	-3	2	8	274	275	5	5	3	-1	9	185	192	3	5	-3	10	22	30	21
2	-3	7	132	148	3	-3	6	7	13	24	13	-2	2	8	362	356	6	6	4	-1	9	54	57	6	-4	-2	10	93	94	3	
3	-3	7	113	117	3	-2	6	7	127	122	3	-1	2	8	442	448	4	4	5	0	9	186	195	3	-3	-2	10	55	44	5	
4	-3	7	183	177	4	-1	6	7	99	99	3	0	0	2	8	85	89	2	2	-5	0	9	177	169	4	-2	-2	10	35	35	7
5	-3	7	0	32	2	-1	-6	8	31	18	10	1	1	2	8	51	55	3	3	-4	0	9	33	24	9	-1	-2	10	187	185	4
5	-3	7	54	55	5	0	0	8	101	97	4	2	2	8	382	384	8	8	0	0	9	37	29	7	1	-2	10	445	434	5	
3	-2	7	81	82	3	-1	-6	8	24	27	13	3	2	8	24	12	19	19	-2	0	9	628	638	6	0	-2	10	0	5	1	
2	-2	7	494	503	6	-2	-6	8	0	11	1	-4	2	8	69	62	5	5	2	-2	9	42	45	3	2	-2	10	94	93	3	
1	-2	7	235	223	3	-3	-5	8	41	38	9	-5	3	8	171	173	4	4	0	0	9	83	85	3	3	-2	10	123	121	3	
0	-2	7	226	219	3	-2	-5	8	0	14	1	-4	2	8	23	6	23	23	4	-1	9	121	125	2	4	-2	10	52	56	6	
0	-2	7	220	236	3	-3	-5	8	0	14	1	-3	3	8	127	126	3	3	2	0	9	45	38	5	5	-2	10	143	133	3	
1	-2	7	136	143	2	-1	-5	8	89	87	2	-4	3	8	235	238	5	5	3	0	9	167	168	3	-5	-1	10	117	119	3	
2	-2	7	262	267	4	0	0	8	48	52	4	-2	1	3	8	544	549	7	7	-4	0	9	0	19	1	-4	-1	10	18	29	18
3	-2	7	78	72	4	1	-5	8	45	44	4	0	0	3	8	331	339	5	5	-6	1	9	208	217	4	-3	-1	10	144	141	3
4	-2	7	0	15	1	2	-5	8	42	44	8	-5	1	3	8	0	9	1	1	-5	1	9	0	5	1	-1	-1	10	59	59	2
5	-2	7	148	146	5	-4	-4	8	39	44	9	-4	4	8	32	41	14	14	-4	1	9	284	285	5	0	-1	10	56	55	2	
5	-2	7	255	247	7	-3	-4	8	125	131	3	-5	4	8	71	71	5	5	-3	1	9	211	214	4	1	-1	10	529	542	7	
3	-1	7	355	339	5	-3	-4	8	143	144	3	-4	4	8	200	205	4	4	-2	1	9	98	104	2	2	-1	10	52	45	5	
2	-1	7	15	5	14	-2	-4	8	0	13	1	-4	4	8	106	106	3	3	1	9	172	165	2	3	-1	10	135	132	2		
1	-1	7	45	40	2	-1	-4	8	16	17	15	-3	4	8	106	106	3	3	0	1	9	91	93	2	4	-1	10	161	157	4	
0	-1	7	735	722	3	0	0	8	148	143	2	-2	1	1	9	40	40	8	8	1	1	9	181	181	2	5	-1	10	128	128	3
0	-1	7	450	445	4	1	-4	8	154	151	2	-1	4	8	54	54	4	4	2	1	9	62	68	5	-6	0	10	43	52	9	
1	-1	7	0	12	1	1	-4	8	114	116	3	0	4	8	136	135	2	2	3	1	9	99	99	3	-5	0	10	84	84	4	
2	-1	7	37	43	7	2	-4	8	109	111	3	2	4	8	168	166	3	3	4	1	9	0	11	1	-4	0	10	54	58	5	
3	-1	7	64	65	4	4	-4	8	0	5	1	-2	4	8	30	31	15	15	-6	2	9	95	95	4	-3	0	10	115	112	2	
4	-1	7	46	43	7	5	-4	8	103	95	4	-5	5	8	42	34	8	8	-5	2	9	55	58	6	-2	0	10	53	44	4	
5	-1	7	168	168	3	-5	-4	8	39	35	10	-4	5	8	116	117	3	3	-4	2	9	89	88	3	-1	0	10	426	434	4	
5	-1	7	126	121	3	-4	-3	8	185	183	4	-3	5	8	167	168	3	3	-3	2	9	200	197	4	0	0	10	418	423	4	
3	0	7	29	3	10	-2	-3	8	128	130	3	-2	5	8	184	187	4	4	-2	2	9	0	12	1	1	0	10	65	65	6	
2	0	7	93	95	5	-3	-3	8	67	79	4	-1	5	8	32	37	12	12	-1	2	9	280	275	10	2	0	10	88	81	3	
1	0	7	356	350	5	0	-3	8	88	91	2	0	0	5	8	191	190	6	6	0	2	9	31	37	6	3	0	10	387	386	8
0	0	7	13	9	12	-1	-3	8	70	61	5	-1	5	8	37	38	7	7	1	2	9	259	274	3	4	0	10	50	49	6	
0	0	7	318	316	9	0	-3	8	155	152	4	-3	6	8	46	42	8	8	2	2	9	139	135	3	-6	1	10	111	114	3	
1	0	7	97	90	1	1	-3	8	50	50	2	-2	6	8	36	44	12	12	5	2	9	190	193	4	-5	1	1				

Table 6. Observed and calculated structure factors for 1

h	k	l	10Fo	10Fc	10s	h	k	l	10Fo	10Fc	10s	h	k	l	10Fo	10Fc	10s	h	k	l	10Fo	10Fc	10s	h	k	l	10Fo	10Fc	10s		
3	3	10	46	53	8	-5	3	11	66	64	5	-4	3	12	79	78	4	-2	4	13	241	227	5	-4	-1	15	85	83	4		
-5	-4	4	145	142	4	-4	3	11	26	11	17	-3	3	12	41	30	7	0	4	13	81	81	5	-3	-1	15	30	24	12		
-4	4	10	433	431	9	-3	3	11	0	24	1	-2	3	12	127	128	3	-1	4	13	140	140	5	-2	-1	15	110	111	3		
-3	4	10	194	184	4	-2	3	11	104	98	3	-1	3	12	86	83	2	0	-5	14	152	154	2	-1	-1	15	223	224	7		
-2	4	10	201	201	4	-1	3	11	280	275	3	0	0	12	180	185	7	1	-5	14	24	39	15	0	0	-1	15	220	219	5	
-1	4	10	344	346	4	0	0	3	11	214	216	3	1	3	12	109	111	2	-2	-4	14	92	94	4	1	-1	15	115	117	3	
0	4	10	44	47	5	1	3	11	98	101	2	2	3	12	10	9	10	-1	-4	14	123	122	2	2	-1	15	184	185	4		
1	4	10	7	13	7	2	2	3	11	210	215	4	-4	4	12	52	44	7	0	-4	14	0	4	1	3	-1	15	132	138	3	
2	4	10	86	80	4	-5	4	11	0	16	1	-3	4	12	63	58	5	1	-4	14	33	20	8	-4	0	15	186	187	4		
-4	5	10	0	0	1	-4	4	11	8	35	8	-2	4	12	54	51	6	-3	-4	14	75	74	5	-3	0	15	236	233	4		
-3	5	10	0	14	1	-3	4	11	223	218	4	-1	4	12	137	133	2	0	-4	14	98	98	3	-2	0	15	7	12	7		
-2	5	10	108	104	3	-2	4	11	95	97	3	0	4	12	85	84	4	-2	-3	14	119	120	3	-1	0	15	42	40	5		
0	5	10	18	25	17	-1	4	11	75	68	4	-1	4	12	83	77	6	-1	-3	14	210	217	3	0	0	15	346	345	9		
1	5	10	12	15	12	0	4	11	109	113	2	-2	5	12	13	7	12	0	-3	14	85	89	2	1	0	15	35	34	10		
1	-6	11	61	61	5	1	4	11	273	273	3	0	-5	13	59	57	4	1	-3	14	118	122	2	2	0	15	0	28	1	1	
-2	-5	11	78	84	5	-3	5	11	105	107	4	0	-5	13	157	162	2	2	-3	14	13	6	12	3	0	15	71	68	5	5	
-1	-5	11	92	92	8	-2	5	11	0	6	1	1	-5	13	96	92	6	3	-3	14	73	78	5	-4	1	15	241	241	5	5	
0	-5	11	169	170	5	-1	5	11	211	210	3	2	-5	13	90	82	4	-4	-2	14	89	97	4	-3	1	15	26	23	17	4	
-1	-5	11	78	72	3	-2	-5	12	9	27	9	-3	-4	13	26	12	19	-3	-2	14	39	29	8	-2	-1	15	223	225	4	4	
-2	-5	11	117	112	3	-1	-5	12	60	60	4	-2	-4	13	138	141	4	-2	-2	14	95	90	3	-1	-1	15	141	135	2	2	
-3	-5	11	194	189	4	0	0	-5	12	0	13	1	-1	-4	13	75	77	3	0	-2	14	11	4	10	0	1	15	112	112	3	3
-4	-4	11	17	3	16	1	-5	12	66	61	3	0	0	-4	13	143	142	2	0	-2	14	261	258	3	-4	-1	15	15	11	15	5
-2	-4	11	87	86	4	2	-5	12	84	83	4	1	-4	13	60	62	4	1	-2	14	187	190	5	2	1	15	98	102	4	6	
0	-4	11	23	11	19	-3	-5	12	73	65	5	2	-4	13	41	21	8	2	-2	14	144	140	3	-3	-2	15	56	56	6	4	
1	-4	11	0	9	1	-3	-4	12	44	31	8	3	-4	13	0	7	1	3	-2	14	88	87	4	-3	2	15	32	38	12	4	
1	-4	11	272	281	4	-1	-4	12	68	65	5	-4	-3	13	0	0	1	-4	-1	14	42	29	7	-2	2	15	136	133	4	5	
2	-4	11	0	24	1	-1	-4	12	43	35	5	-3	-3	13	110	111	4	-3	-1	14	74	65	4	-1	2	15	277	273	5	5	
3	-4	11	150	149	3	0	-4	12	112	114	2	-2	-3	13	80	79	4	-2	-1	14	254	259	5	0	2	15	94	95	2	10	
4	-4	11	67	66	5	1	-4	12	269	268	4	-1	-3	13	32	34	13	-1	-1	14	62	65	3	-4	3	15	108	110	10	4	
-4	-3	11	49	50	7	2	-4	12	77	76	4	0	-3	13	41	43	5	0	-1	14	35	45	9	-4	3	15	88	75	4	4	
-3	-3	11	201	193	4	3	-4	12	103	104	3	2	-3	13	78	75	2	1	-1	14	118	116	2	-3	3	15	117	120	3	7	
-2	-3	11	136	141	3	-4	-3	12	67	71	5	3	-3	13	33	31	11	3	-1	14	205	206	4	-2	3	15	46	46	7	3	
-1	-3	11	307	315	3	-3	-3	12	100	97	3	3	-3	13	66	66	5	3	-1	14	0	15	1	-1	3	15	47	42	5	5	
0	-3	11	327	324	13	-2	-3	12	32	30	10	-4	-3	13	98	101	4	-5	0	14	141	147	3	0	3	15	171	174	2	2	
-1	-3	11	143	145	2	-1	-3	12	33	35	9	-4	-2	13	160	156	3	-4	0	14	167	159	4	-1	-4	16	26	2	11	1	
-2	-3	11	165	173	4	0	0	-3	12	60	57	5	-3	-2	13	97	98	3	-3	0	14	0	3	1	0	-4	16	0	29	1	1
-3	-3	11	77	83	4	1	-3	12	78	78	3	-2	-2	13	78	80	4	-2	0	14	166	173	3	-1	-4	16	28	30	10	4	
-4	-4	11	54	46	6	2	-2	-3	12	294	284	5	-1	-2	13	195	198	3	-1	0	14	56	54	4	-2	-3	16	32	29	13	3
-5	-4	11	145	144	3	3	-3	12	62	70	5	0	-2	13	183	178	2	0	0	14	159	161	2	-1	-3	16	78	79	3	3	
-4	-4	11	88	90	4	4	-3	12	179	180	4	2	-2	13	51	52	4	1	0	14	187	183	5	0	-3	16	16	16	16	6	6
-3	-4	11	142	147	3	-4	-2	12	106	115	3	2	-2	13	45	42	7	2	0	14	72	74	5	0	-3	16	37	39	6	6	
-2	-4	11	184	191	4	-3	-2	12	29	24	12	3	-2	13	69	67	4	3	0	14	62	65	5	-2	-3	16	34	27	12	4	
-1	-4	11	357	356	11	-2	-2	12	109	103	3	4	-2	13	91	87	4	-5	1	14	141	141	3	-3	-2	16	169	167	4	4	
0	-4	11	141	139	2	-1	-2	12	97	92	2	-5	-1	13	40	38	9	-4	1	14	117	110	3	-2	-2	16	130	132	4	5	
1	-4	11	94	98	3	0	0	-2	12	261	261	3	-4	-1	13	64	65	5	-3	1	14	65	58	4	0	-2	16	47	46	5	5
2	-4	11	76	79	4	1	-2	12	107	105	2	-3	-1	13	169	176	3	-2	-1	14	112	115	3	-1	-2	16	17	18	17	4	
3	-4	11	65	71	5	2	-2	12	22	16	22	-2	-1	13	31	37	10	-1	1	14	24	21	23	1	-2	16	92	95	3	6	
4	-4	11	30	38	14	3	-2	12	111	113	3	0	-1	13	372	375	8	0	0	14	54	57	6	2	-2	16	58	58	6	3	
-5	-5	11	103	102	3	4	-2	12	197	199	4	1	-1	13	52	49	4	1	1	14	64	67	3	-4	-1	16	87	94	5	5	
-4	-5	11	21	21	20	-5	-1	12	62	66	6	2	-1	13	57	58	4	2	1	14	126	123	3	-3	-1	16	56	53	6	4	
-3	-5	11	278	284	5	-4	-1	12	68	66	4	2	-1	13	202	187	4	3	1	14	0	2	1	-2	-1	16	91	91	4	4	
-2	-5	11	218	221	4	-3	-1	12	152	157	3	3	-1	13	131	129	3	-5	2	14	114	113	4	-1	-1	16	123	119	2	8	
-1	-5	11	106	106	2	-2	-1	12	363	384	7	-4	-1	13	44	31	8	-4	2	14	55	53	6	0	-1	16	31	36	6	6	
0	-5	11	188	189	1	-1	-1	12	65	59	2	-5	0	13	164	165	3	-3	2	14	124	124	3	1	-1	16	41	42	6	6	
1	-5	11	19	0	18	0	0	-1	12	26	19	7	-4	0	13	222	218	4	-2	2	14	77	78	4	-2	-1	16	61	54	6	4
2	-5	11	33	44	10	1	-1	12	147	154	4	-3	0	13	46	50	6	-1	2	14	73	73	6	-4	0	16	81	77	4	6	
3	-5	11	29	17	12	2	-1	12	146	143	3	-2	0	13	68	61	4	0	2	14	183	179	4	-3	0	16	62	68	5	5	
4	-5	11	72	82	5	3	-1	12	89	82	3	-1</																			

Table 6. Observed and calculated structure factors for 1

Observed						Calculated						Observed						Calculated											
h	k	l	10Fo	10Fc	10s	h	k	l	10Fo	10Fc	10s	h	k	l	10Fo	10Fc	10s	h	k	l	10Fo	10Fc	10s						
1	-1	17	93	95	3	1	0	17	78	77	3	-3	2	17	75	69	5	-2	-1	18	38	34	10	0	0	18	1	14	1
2	-1	17	78	73	5	-3	1	17	0	27	1	-2	2	17	41	34	9	-1	-1	18	49	39	5	-2	1	18	41	40	9
-3	0	17	93	94	4	-2	1	17	228	218	4	-1	2	17	100	100	5	0	-1	18	162	163	5	-1	1	18	164	160	2
-2	0	17	77	78	4	-1	1	17	0	0	1	0	2	17	35	12	8	1	-1	18	0	13	1	0	1	18	117	115	2
-1	0	17	28	36	10	0	1	17	26	13	11	-1	-2	18	54	50	4	-2	0	18	45	32	8						
0	0	17	146	142	3	1	1	17	39	51	7	0	-2	18	53	48	5	-1	0	18	120	121	2						